Case Study II 14:20-15:20

First-Principles Study of Thermoelectric Transport in Magnetic Materials with Machine Learning Analysis of the Anomalous Hall Effect

NanoMaRi

Fumiyuki Ishii
Nanomaterials Research Institute,
Kanazawa University, Japan


日本
JAPAN
N
北海道
青森
秋田
岩手
山形
宮城
新潟
福島
Kanazawa
石川
富山
長野
群馬
栃木
福井
茨城
埼玉
Kyoto
岐阜
山梨
東京
Tokyo
島根
鳥取
岡山
兵庫
京都
滋賀
愛知
静岡
神奈川
千葉
山口
広島
大阪
福岡
佐賀
香川
徳島
Osaka
奈良
三重
長崎
大分
愛媛
高知
熊本
和歌山
宮崎
鹿児島
沖縄
© CyberMap Japan Corp.

Group Member in My Lab

Teure-track Assistant Professor
Dr. Naoya Yamaguchi (NanoMaRi)

Research Assistant Professor
Dr. Hana Pratiwi Kadarisman (NanoMaRi, KU Promising Researcher)

Postdoctoral Researcher
Zhang Yaotang

Students(2025.4.1)
D3 Shohei Miura (HaKaSe+)
D3 Salsabila Amanda Putri (GHR)
D2 Yedija Yusua Sibuea Teweng (HaKaSe+)
D2 Yang Jingwen
D2 Zohan Syah Fatomi (e-ASIA)
D2 Ahmad Sohib (GHR)
D2 Putri Syifa Fauzia Hariyanti (HaKaSe+)
D1 Ahmad Al Ghiffari (HaKaSe+)
D1 Ahmed Muhammad (GHR)
D1 Jin Inoue
M2 Muhammad Rosyid Ridho (GHR)
M2 Nadia Maharani Chadiza (GHR)
M2 Adzky Mathla Syawly (DDP, ITB)
M2 David Bandhaso (DDP, UGM)
M2 Vani Sugiyono (DDP, UGM)
M2 Shigetomo Yanase
M2 Sota Yamate
M2 Arifia Pratiwi Nugraheni (DDP, UGM)
M1 Sarah Auliyaurrohman Setiawati Sukoco (GHR)
M1 Md Joynadul Hosain Sakib (GHR)
M1 Nur Anggita Sari (GHR)
M1 Shota Sasajima
M1 Yang Yue
B4 Yuma Nakamura

28 members
15 Indonesia
8 Japan
3 China
1 Bangladesh
1 Pakistan

Importance of Thermoelectricity

Energy / Environmental issues

- Need for eco-friendly energy sources
- Need for the reduction of CO_2 emission

One good aid: **Thermoelectric (TE) conversion**

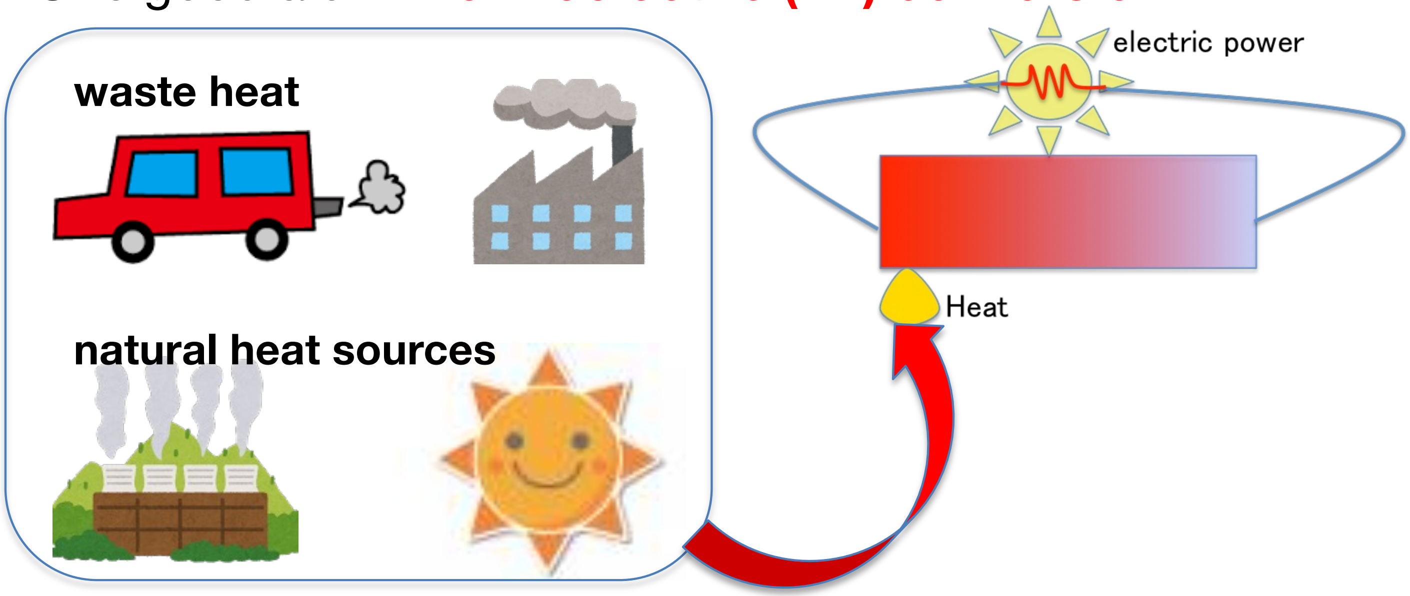

Studies of thermoelectricity contribute to SDGs (Sustainable Development Goals)

The Role of Physics in Supporting Sustainable Development Goals

Waste Heat

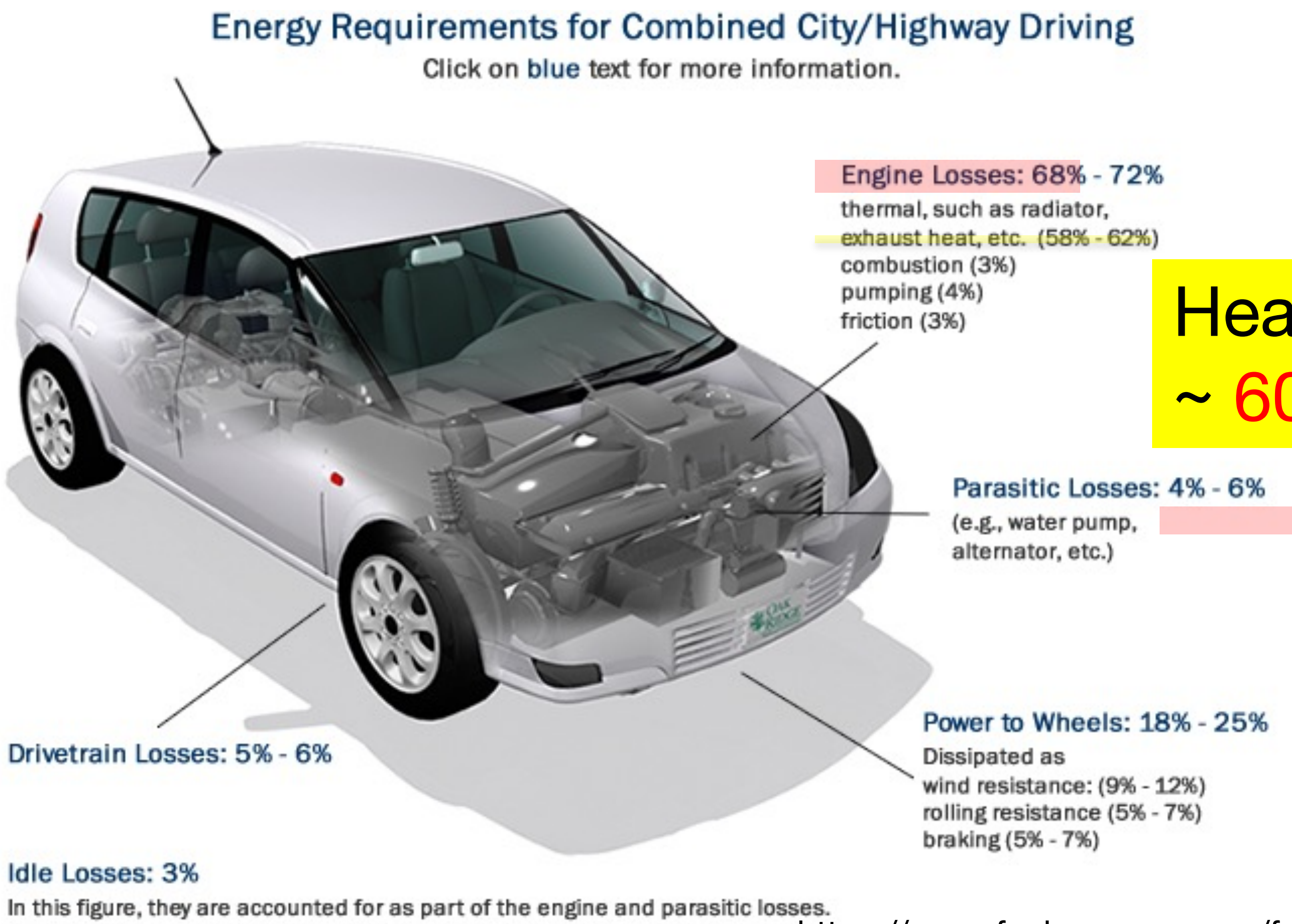

Heat loss

~ 60 %

https://www.fueleconomy.gov/feg/atv.shtml

Collaborative research, 2022-2024

Data-driven computational design of high-performance thermoelectrics in atomic layers and topological materials

This cooperative research project aims to achieve high-performance thermoelectrics based on two-dimensional atomic layers and topological materials using cutting-edge computational tools assisted by experimental data. By this integrated approach, the project may give better thermoelectric materials design that will contribute to understanding both conventional and exotic thermoelectric materials as well as to the development of new thermoelectric applications.

Goal of the project

- **Achieving ZT>2 in 2D and topological materials**
- **Generating more than 10,000 thermoelectric data sets for database**

Thermoelectric figure of merit ZT

$$ZT = \frac{X^2\sigma}{\kappa_l + \kappa_e} T$$

$X = S, N$: Seebeck or Nernst coefficient

σ : Electric conductivity

κ_l, κ_e : Lattice , electronic thermal conductivity

T : Temperature

Present ZT

Y. Sun et al., Front. Chem., **10**, 865281(2022).

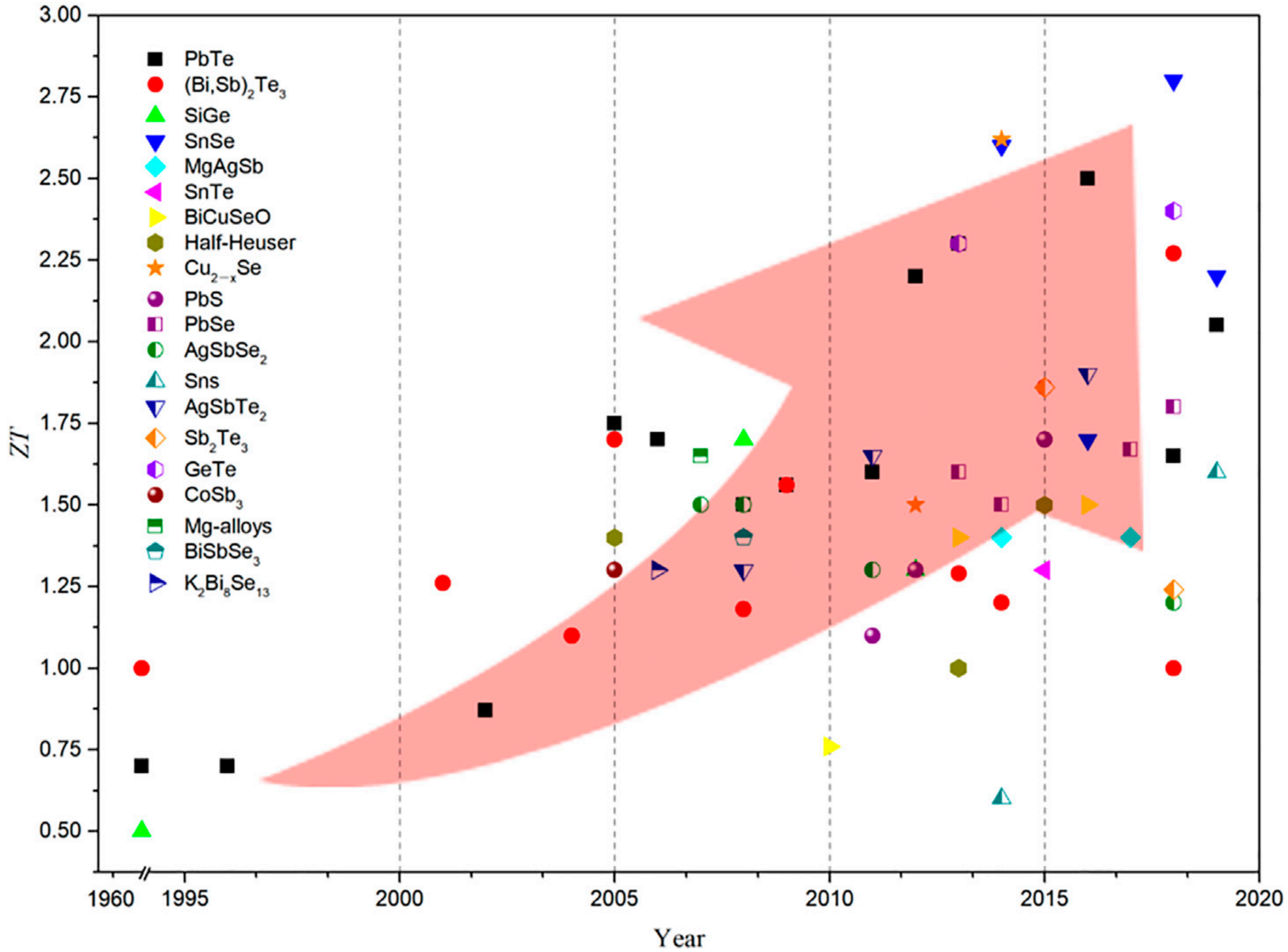

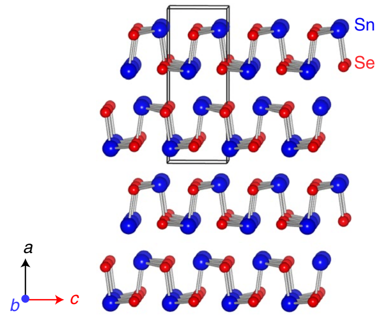

vdW SnSe

In Seebeck effect, ZT > 2 has already been achieved, but it occurs at high temperatures (600-800K), and in many systems, ZT < 1 at room temperature (300K) (e.g., SnSe). Since N/S < 1/100, the ZT of Nernst effect is less than 1/10000 of that of Seebeck effect. Example calculations:

- CoMnSb: ZNT ~ 6x10^-5 (490K)
- MnBi2Te4: ZNT ~ 1.5x10^-3 (20K)

Thermoelectric properties of topological materials?

The Nobel Prize in Physics 2016

© Trinity Hall, Cambridge University. Photo: Kiloran Howard

David J. Thouless

Prize share: 1/2

Photo: Princeton University, Comms. Office, D. Applewhite

F. Duncan M. Haldane

Prize share: 1/4

Ill: N. Elmehed. © Nobel Media 2016

J. Michael Kosterlitz

Prize share: 1/4

The Nobel Prize in Physics 2016 was divided, one half awarded to David J. Thouless, the other half jointly to F. Duncan M. Haldane and J. Michael Kosterlitz *"for theoretical discoveries of topological phase transitions and topological phases of matter"*.

Topology

The properties of a geometric object that are preserved under continuous deformations

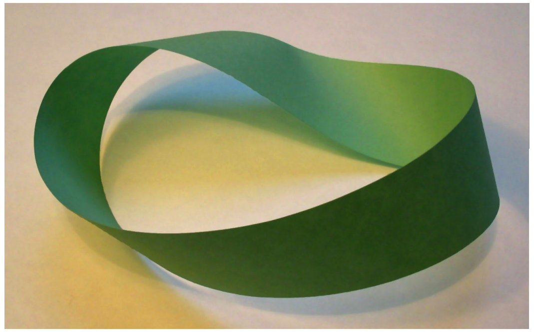

Möbius strips

Mug into a doughnut (torus)

It is characterized by topological index.

Cow into a sphere

en.wikipedia

Topology
Gauss-Bonnet Theorem

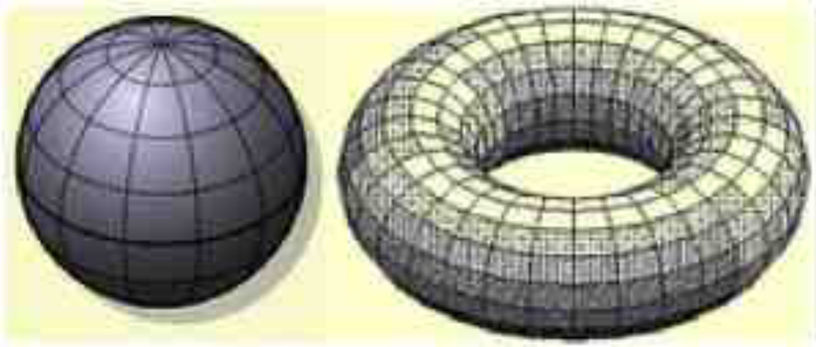

$g = 0$ $g = 1$ $g = 1$ $g = 2$

Gaussian curvature: $\boldsymbol{\Omega} = \det \begin{pmatrix} \frac{\partial^2 z}{\partial x^2} & \frac{\partial^2 z}{\partial x \partial y} \\ \frac{\partial^2 z}{\partial y \partial x} & \frac{\partial^2 z}{\partial y^2} \end{pmatrix}$

The Hessian at the tangent plane

$$\boxed{\frac{1}{2\pi} \int_S d\sigma \, \boldsymbol{\Omega} = 2(1 - g)}$$

R. Resta, Lecture note at Univ. Trieste

g is non-negative integer.

Hall conductivity and Chern number

(Thouless, Kohmoto, Nightingale, den Nijs, 1982)

$$\psi_{\boldsymbol{k}}(\boldsymbol{r}) = e^{i\boldsymbol{k}\cdot\boldsymbol{r}} u_{\boldsymbol{k}}(\boldsymbol{r})$$

$$\sigma_{\mathrm{H}} = \frac{ie^2}{2\pi h}\sum\int d^2k \int d^2r \left(\frac{\partial u^*}{\partial k_1}\frac{\partial u}{\partial k_2} - \frac{\partial u^*}{\partial k_2}\frac{\partial u}{\partial k_1}\right)$$

$$= \frac{ie^2}{4\pi h}\sum\oint dk_j \int d^2r \left(u^*\frac{\partial u}{\partial k_j} - \frac{\partial u^*}{\partial k_j}u\right),$$

※ For any insulator or isolated band,

$$\sigma_H = C\frac{e^2}{h}$$

C: Chern number

$$\sigma_{ij} \equiv \sigma_H (i \neq j)$$

Chern number contributes to thermoelectric effect in Magnet

Progress of Berry phase theory in the physics of ferroelectrics and topological insulator

$$\psi_{\boldsymbol{k}}(\boldsymbol{r}) = e^{i\boldsymbol{k}\cdot\boldsymbol{r}}\underline{u_{\boldsymbol{k}}(\boldsymbol{r})}$$

$$\boldsymbol{A}_n(\boldsymbol{k}) = i\langle u_{n\boldsymbol{k}}|\boldsymbol{\nabla}_{\boldsymbol{k}}|u_{n\boldsymbol{k}}\rangle$$

Berry connection
→ Electric polarization in insulators

$$\boldsymbol{\Omega}_n(\boldsymbol{k}) = \boldsymbol{\nabla}_{\boldsymbol{k}} \times \boldsymbol{A}_n(\boldsymbol{k})$$

Berry curvature
→ Anomalous Hall conductivity

$$\boldsymbol{v}_n(\boldsymbol{k}) = \frac{1}{\hbar}\frac{\partial \varepsilon_n(\boldsymbol{k})}{\partial \boldsymbol{k}} - \frac{e}{\hbar}\boldsymbol{E} \times \boldsymbol{\Omega}_n(\boldsymbol{k})$$

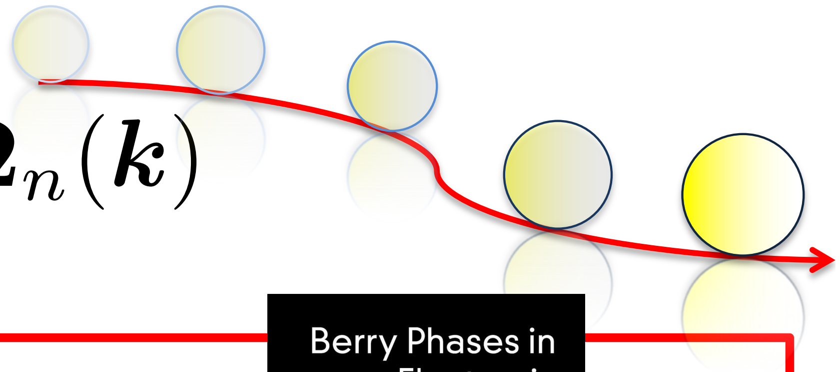

- Electric polarization in insulators, RMP, **66**,899(1994)
- Anomalous Hall effect and related issues, RMP, **82**,1539(2010), **82**,1959(2010)
- Topological insulators, RMP, **82**, 3045(2010)
- Weyl and Dirac semimetals, RMP, **90**, 015001(2018)

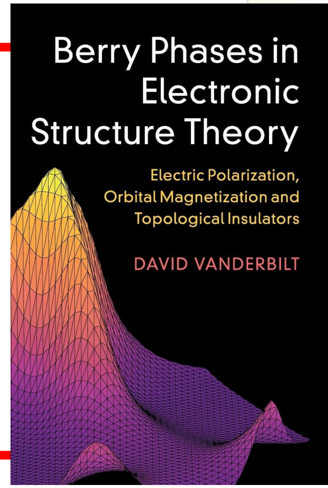

Code development

Main developer : T. Ozaki
(ISSP, Univ. of Tokyo)

OpenMX Open source package for Material eXplorer

O(N) density functional code
GNU-GPL http://www.openmx-square.org

Features

Local atomic basis

Capabilities

MD

- Electric polarization (Berry Phase)
  Comput. Phys. Commun. 280, 108487 (2022) New
- Z_2 topological invariant
  (1)Parity, (2)Fukui-Hatsugai,
  (3) Soluyanov-Vanderbilt, Wilson loop Hybrid Wannier Function
- Chern number (Berry Curvature)
- Finite electric field (Berry phase)
- Interface with Wannier90 New
- Anomalous Hall Conductivity Phys. Rev. B 107, 024404(2023)

Implementation of Fukui-Hatsugai-Suzuki Methods in OpenMX

Phys. Rev. B 107, 024404(2023)

$$\Omega(\mathbf{k}) = (\nabla \times \mathbf{A})_z$$
$$= A_{k_y}(\mathbf{k} + \Delta k_x) - A_{k_y}(\mathbf{k}) - (A_{k_x}(\mathbf{k} + \Delta k_y) - A_{k_x}(\mathbf{k}))$$

$$\mathbf{A}_\mu(\mathbf{k}) = \mathrm{Im}\log U_\mu(\mathbf{k})$$
$$U_\mu(\mathbf{k}) = \langle u(\mathbf{k}) | u(\mathbf{k} + \Delta\mu)\rangle$$

$$U_{ab} = N^{-1} \det\langle u_a | u_b \rangle$$

$$\Omega(\mathbf{k}) = \mathrm{Im}\log U_{12}U_{23}U_{34}U_{41}$$
$$C = \sum_{\mathrm{BZ}} \Omega(\mathbf{k})$$

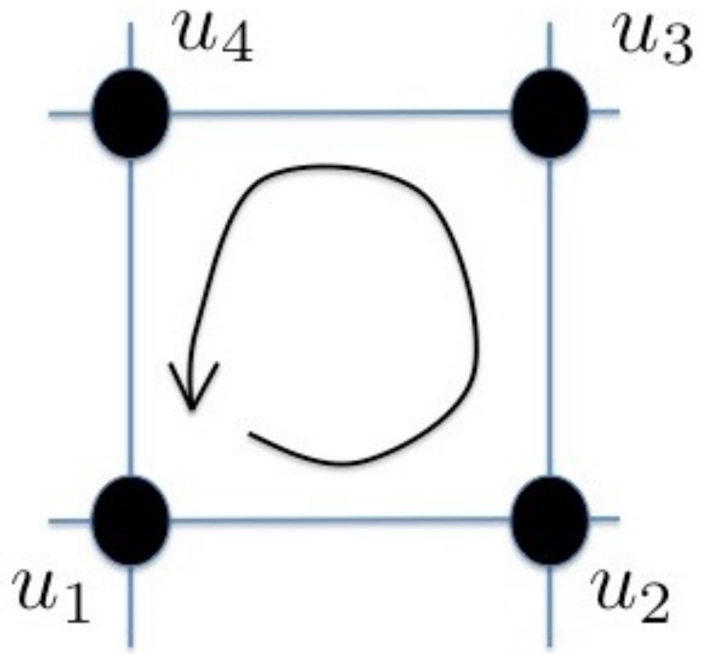

T. Fukui, Y. Hatsugai, and H. Suzuki, J. Phys. Soc. Jpn. **74**, 1674 (2005).

Data-driven computational design

金沢大学 KANAZAWA UNIVERSITY

Prediction, exploration, and design of physical properties through material simulation

Materials informatics, high-throughput calculations

Kohn-Sham Eq.

$$[-\Delta + v_{eff}(n(r))]\psi_i(r) = \varepsilon_i \psi_i(r)$$

↓ Wavefunctions, energies

$$n(r) = \sum_{i=1}^{N} |\psi_i(r)|^2$$ Charge density

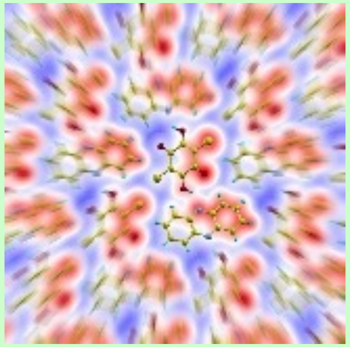

↓ Effective potential

$$v_{eff}(n(r)) = -\sum_n \frac{Z_n e^2}{|r - R_n|} + \frac{e^2}{2}\int \frac{n(r)n(r')}{|r - r'|} dr dr' + \mu_{xc}(r)$$

Ex. Iron compounds high magneto-thermoelectric effects

Fe_xM_y

(determination of element M, composition x,y)

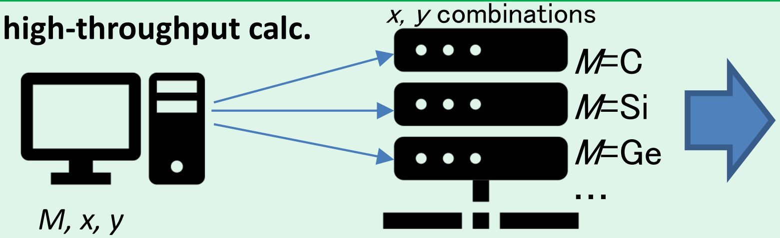

Nature **581**, 53–57(2020)

World's best at room temperature and zero magnetic field Realizing the magneto-thermoelectric effect Discovery of iron-based materials

KU, RIKEN, UT

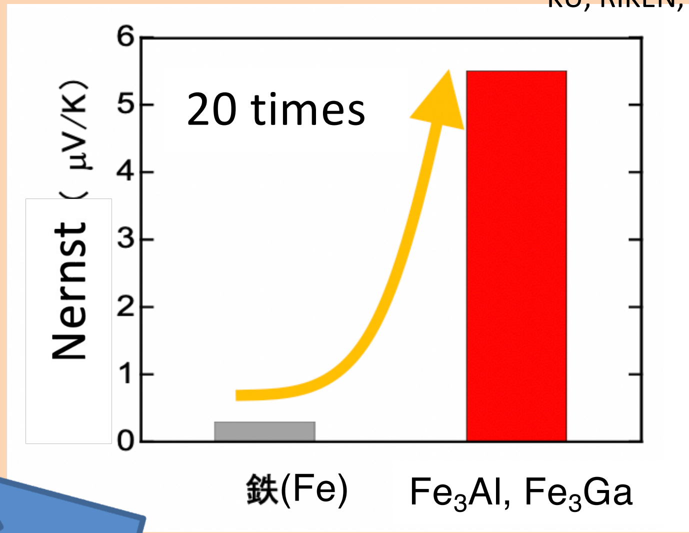

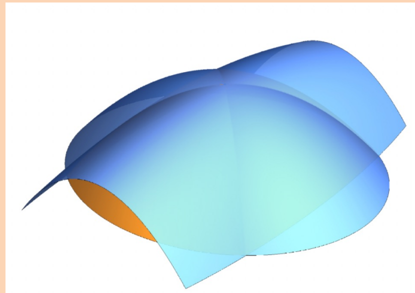

Topological properties that contribute to high thermoelectricity electronic state (called nodal web)

Article

Iron-based binary ferromagnets for transverse thermoelectric conversion

https://doi.org/10.1038/s41586-020-2230-z

Received: 26 July 2019

Accepted: 4 February 2020

Published online: 27 April 2020

Check for updates

Akito Sakai[1,2,3,10], Susumu Minami[4,5,10], Takashi Koretsune[6,10], Taishi Chen[1,3,10], Tomoya Higo[1,3,10], Yangming Wang[1], Takuya Nomoto[7], Motoaki Hirayama[5], Shinji Miwa[1,3,8], Daisuke Nishio-Hamane[1], Fumiyuki Ishii[4,5], Ryotaro Arita[3,5,7] & Satoru Nakatsuji[1,2,3,8,9]✉

Thermoelectric generation using the anomalous Nernst effect (ANE) has great potential for application in energy harvesting technology because the transverse geometry of the Nernst effect should enable efficient, large-area and flexible coverage of a heat source. For such applications to be viable, substantial improvements will be necessary not only for their performance but also for the associated material costs, safety and stability. In terms of the electronic structure, the anomalous Nernst effect (ANE) originates from the Berry curvature of the conduction electrons near the Fermi energy[1,2]. To design a large Berry curvature, several approaches have been considered using nodal points and lines in momentum space[3–10]. Here we perform a high-throughput computational search and find that 25 percent doping of aluminium and gallium in alpha iron, a naturally abundant and low-cost element, dramatically enhances the ANE by a factor of more than ten, reaching about 4 and 6 microvolts per kelvin at room temperature, respectively, close to the highest value reported so far. The comparison between experiment and theory indicates that the Fermi energy tuning to the nodal web—a flat band structure made of interconnected nodal lines—is the key for the strong enhancement in the transverse thermoelectric coefficient, reaching a value of about 5 amperes per kelvin per metre with a logarithmic temperature dependence. We have also succeeded in fabricating thin films that exhibit a large ANE at zero field, which could be suitable for designing low-cost, flexible microelectronic thermoelectric generators[11–13].

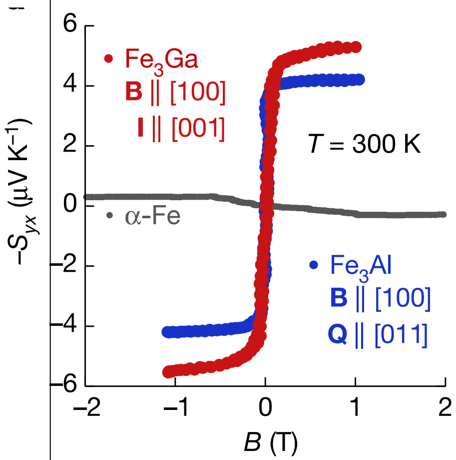

c

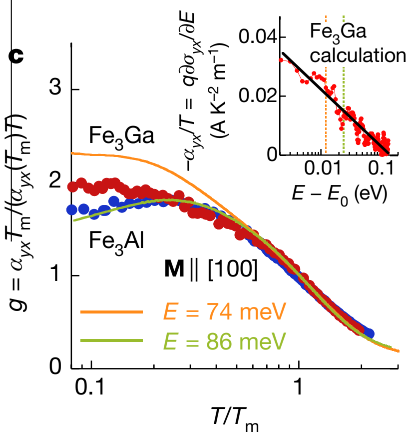

Temperature gradient ∇T driven electric current

$$\mathbf{j} = \tilde{\sigma}\mathbf{E} + \tilde{\alpha}(-\nabla T)$$

Conductivity tensor

Thermoelectric tensor

$$\begin{pmatrix} j_x \\ j_y \end{pmatrix} = \begin{pmatrix} \sigma_{xx} & \sigma_{xy} \\ \sigma_{yx} & \sigma_{yy} \end{pmatrix} \begin{pmatrix} E_x \\ E_y \end{pmatrix} - \begin{pmatrix} \alpha_{xx} & \alpha_{xy} \\ \alpha_{yx} & \alpha_{yy} \end{pmatrix} \begin{pmatrix} \nabla_x T \\ 0 \end{pmatrix}$$

Anomalous Hall effect (AHE): Integration of Berry curevature (local Berry phase in B.Z.)

$$\sigma_{xy}(\varepsilon) = -\frac{e^2}{\hbar}\sum_{n,\mathbf{k}} \Omega^z_{n,\mathbf{k}}\Theta(\varepsilon - \varepsilon_{\mathbf{k}})$$

Berry curvature contributes to thermoelectric effect in Magnet

Thermoelectric Effect

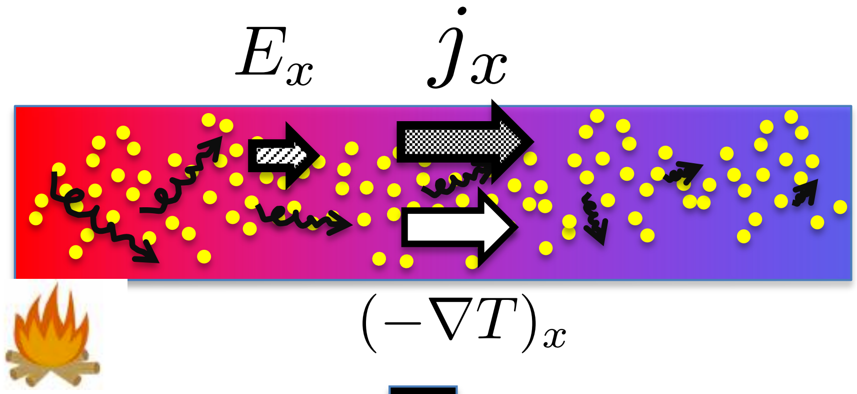

$$\mathbf{j} = \tilde{\sigma}\mathbf{E} + \tilde{\alpha}(-\nabla T)$$

1. Electrons relax into cooler region.
2. Electric field is induced along x-direction E_x
3. System becomes stationary $j_x = 0$

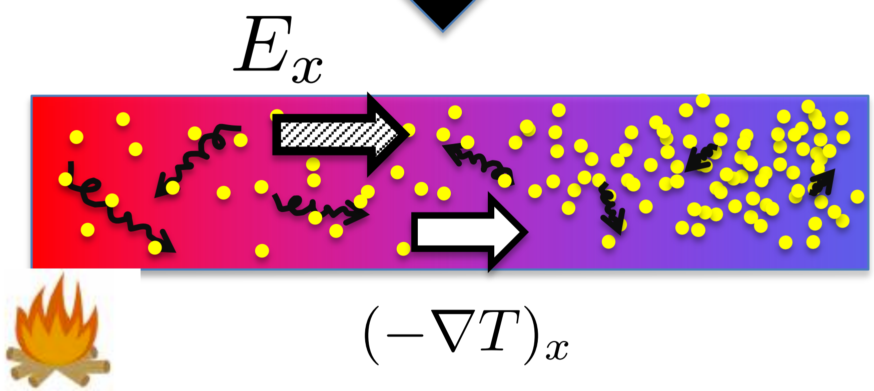

Seebeck coefficient

$$S \equiv \frac{E_x}{(\nabla T)_x} = \frac{\alpha_{xx}}{\sigma_{xx}}$$

Thermoelectric Effect in ***MAGNET***

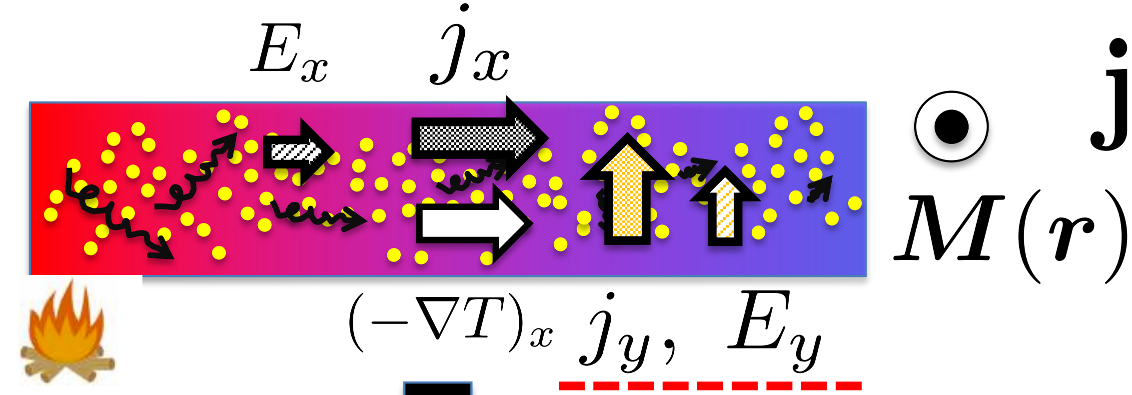

$$\mathbf{j} = \tilde{\sigma}\mathbf{E} + \tilde{\alpha}(-\nabla T)$$

- Electrons relax into cooler region.
- Electric field is induced E_x & E_y
- System becomes stationary $j_x = j_y = 0$

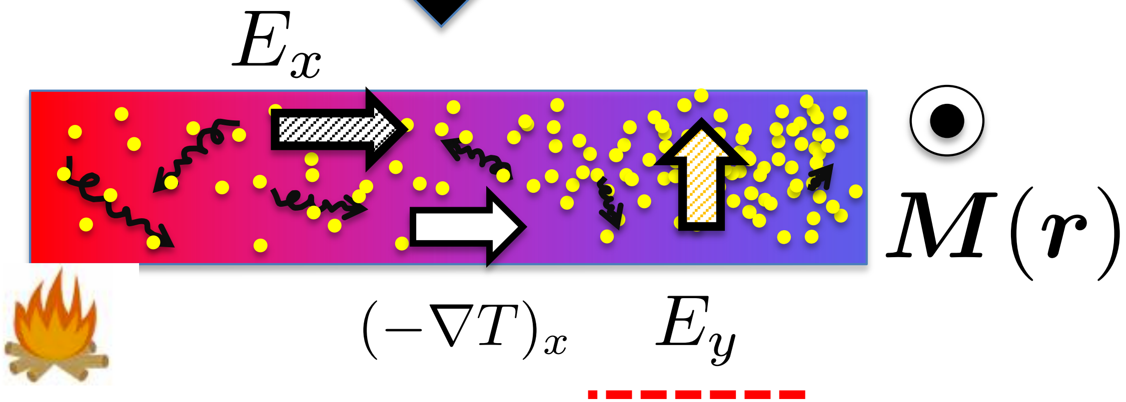

Nernst coefficient

$$N \equiv \frac{E_y}{\nabla T_x} = \frac{\alpha_{xy}}{\sigma_{xx}}$$

Conductivities ⇒ Nernst coef.

	electric field	temperature gradient
charge current :	$$\mathbf{j} = \tilde{\sigma}\mathbf{E} + \tilde{\alpha}(-\nabla T)$$	

open circuit condition $\mathbf{j} = 0$

$$\Rightarrow \quad \mathbf{E} = -\begin{pmatrix} \sigma_{xx} & \sigma_{xy} \\ \sigma_{yx} & \sigma_{yy} \end{pmatrix}^{-1} \begin{pmatrix} \alpha_{xx} & \alpha_{xy} \\ \alpha_{yx} & \alpha_{yy} \end{pmatrix} (-\nabla T)$$

$$N \equiv \frac{E_y}{(\nabla T)_x} = \frac{N_0}{1 + r_H^2} - \frac{r_H S_0}{1 + r_H^2}$$

pure Nernst coeff.

$$N_0 \equiv \frac{\alpha_{xy}}{\sigma_{xx}}$$

Hall angle ratio

$$r_H \equiv \frac{\sigma_{xy}}{\sigma_{xx}}$$

pure Seebeck coeff.

$$S_0 \equiv \frac{\alpha_{xx}}{\sigma_{xx}}$$

Conductivities ⇒ Nernst coef.

$$N = \frac{N_0}{1 + r_H^2} - \frac{r_H S_0}{1 + r_H^2}$$

pure Nernst coeff.

$$N_0 \equiv \frac{\alpha_{xy}}{\sigma_{xx}}$$

Hall angle ratio

$$r_H \equiv \frac{\sigma_{xy}}{\sigma_{xx}}$$

pure Seebeck coeff.

$$S_0 \equiv \frac{\alpha_{xx}}{\sigma_{xx}}$$

Relation between (*thermally* induced current ∝ α) & (*electrically* induced current ∝ σ)

$$\alpha_{ij} = \frac{k_B}{e} \int d\varepsilon [\sigma_{ij}(\varepsilon)]_{T=0} \left(\frac{\varepsilon - \mu}{k_B T} \right) \left(-\frac{\partial f}{\partial \varepsilon} \right)$$

$$\sigma_{ij} = \int d\varepsilon [\sigma_{ij}(\varepsilon)]_{T=0} \left(-\frac{\partial f}{\partial \varepsilon} \right)$$

All we need to know

$[\sigma_{ij}(\varepsilon)]_{T=0}$ **Energy (ε)-dependence of conductivities at zero temperature**

Y. P. M. & F. Ishii, Sci. Rep. **6,** 28076 (2016). JPS Conf. Proc. **3**, 017035(2014), ibid. **5**, 011023 (2015).

Applications
Part I

①Half-Heusler Alloy CoMnSb

- S. Minami, **FI**, Y.P. Mizuta and M. Saito,
  Appl. Phys. Lett. **113**, 032403 (2018).

② Fe_3X(X=*Al*, *Ga*)

Sakai, S. Minami, T. Koretsune, T. Chen, T. Higo, Y. Wang, T. Nomoto, M. Hirayama, S. Miwa, D. Nishio-Hamane, **FI**, R. Arita and S. Nakatsuji,
Nature **581**, 53-57 (2020).

Questions to be solved

1. Which contribution is dominant in real materials?
2. What is the key to enhance Nernst coefficients?
3. Can we predict the behavior of Nernst effect ?

$$N = \frac{N_0}{1 + r_H^2} - \frac{r_H S_0}{1 + r_H^2}$$

∇T induced Anomalous Hall Effect

Seebeck current contribution

Application ①: Half-Heusler alloy

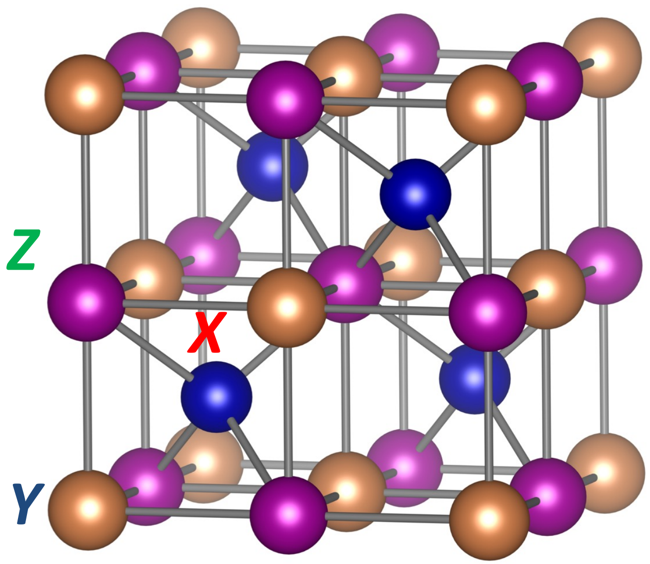

C1$_b$ –type ($F\bar{4}3m$)

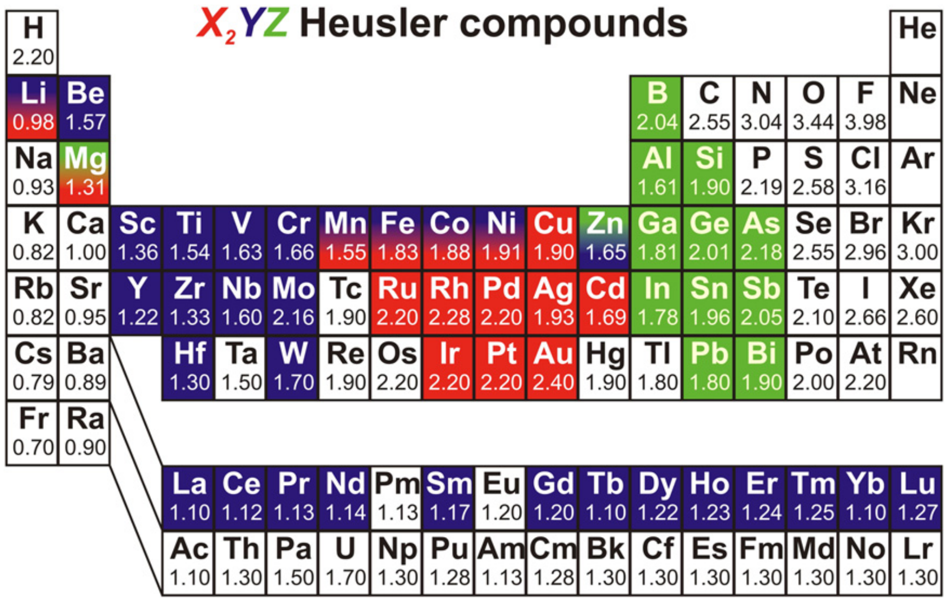

Combination of the elements for Heusler alloy

Physical properties of (half) Heusler alloy

·Narrow gap semiconductor ·Spin gapless semiconductor
·Ferromagnetic(Half-metal) ·Antiferromagnetic
·Semimetal ·Topological insulator

Co*M*Sb (*M*=Sc-Mn)

M	a (Å)	$a_{exp.}$ (Å)	a_{calc} (Å)	n_v	T_C (K)
Sc	6.06	…	6.09	17	…
Ti	5.88	5.88	5.88	18	…
V	5.80	5.80	5.81	19	58
Cr	5.79	…	5.79	20	…
Mn	5.87	5.87	5.82	21	490

Large Seebeck coefficient S_0 is reported for doped CoTiSb

$$N = \frac{N_0}{1+r_H^2} - \frac{\boxed{r_H S_0}}{1+r_H^2}$$

Band structure and DOS of CoMnSb

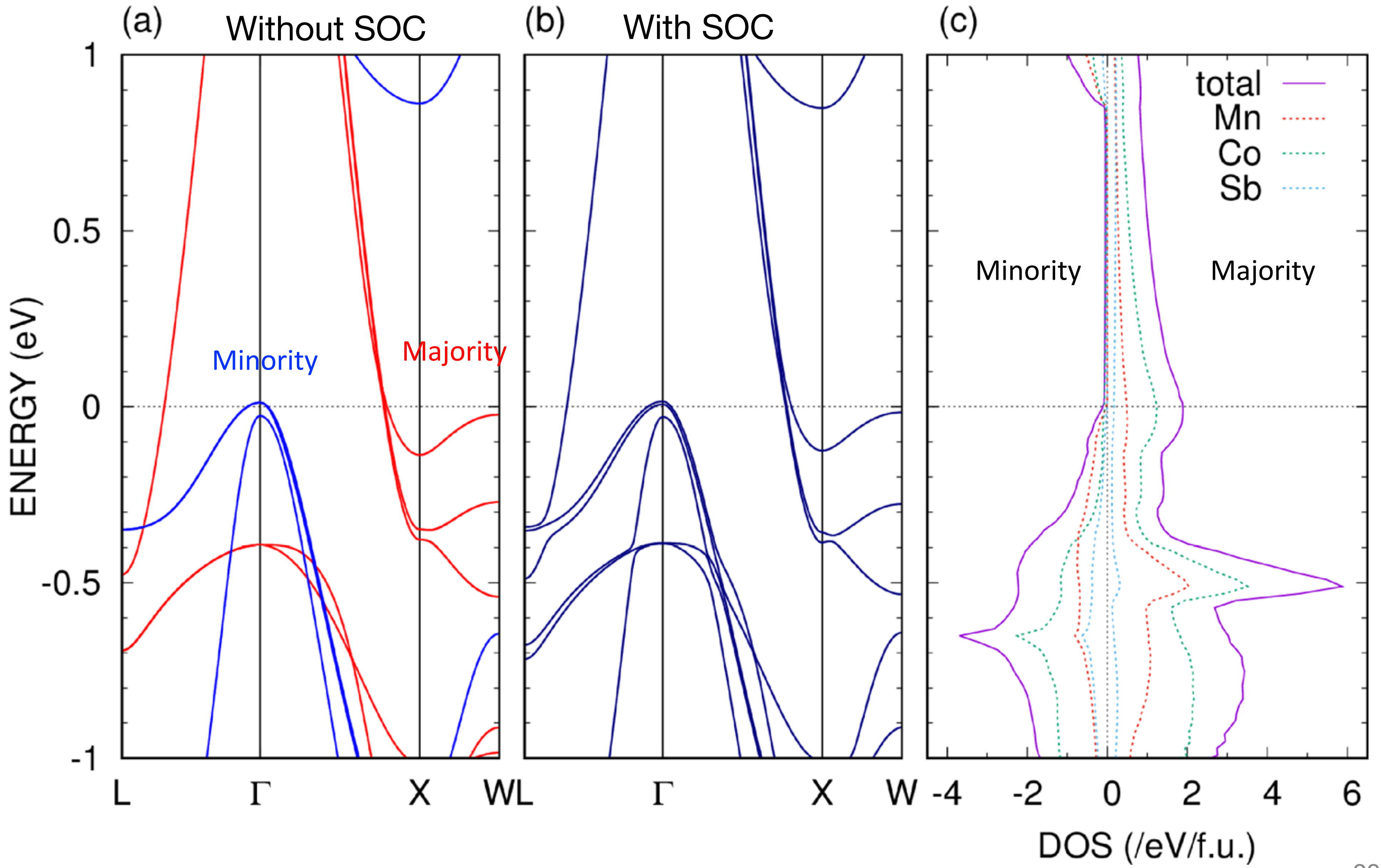

Seebeck and Nernst coefficient in CoMnSb

Each component of calculated thermoelectric coefficients (μV/K), Hall angle ratio, and evaluated relaxation time (fs) for CoMnSb at Fermi energy($\mu = 0$).

Temperature(K)	S_0	N_0	$r_H[\times 10^{-2}]$	S	N	τ
100	- 5.80	-0.11	-0.42	-5.79	-0.13	7.0
300	-16.00	-0.85	-1.02	-15.99	-1.02	2.9

$$N = \frac{N_0}{1+\cancel{r_H^2}} - \cancel{\frac{r_H S_0}{1+r_H^2}}$$

$$N \simeq N_0$$

$$N_0 \propto \alpha_{xy} \propto \boxed{\frac{\mathrm{d}\sigma_{xy}(\varepsilon)}{\mathrm{d}\varepsilon}}$$

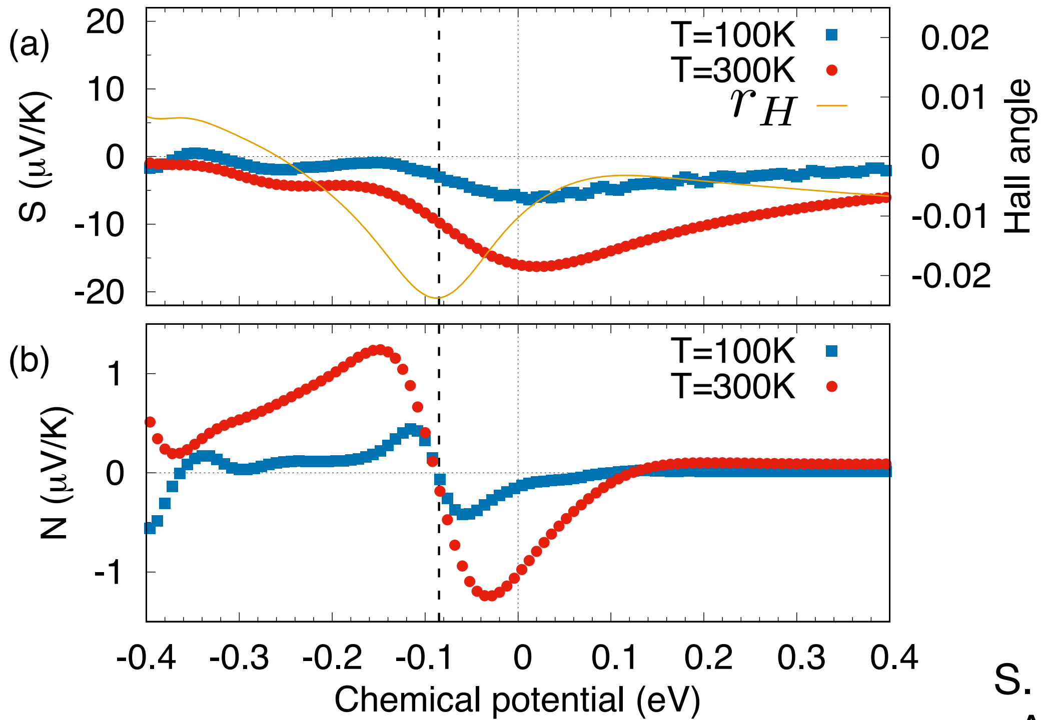

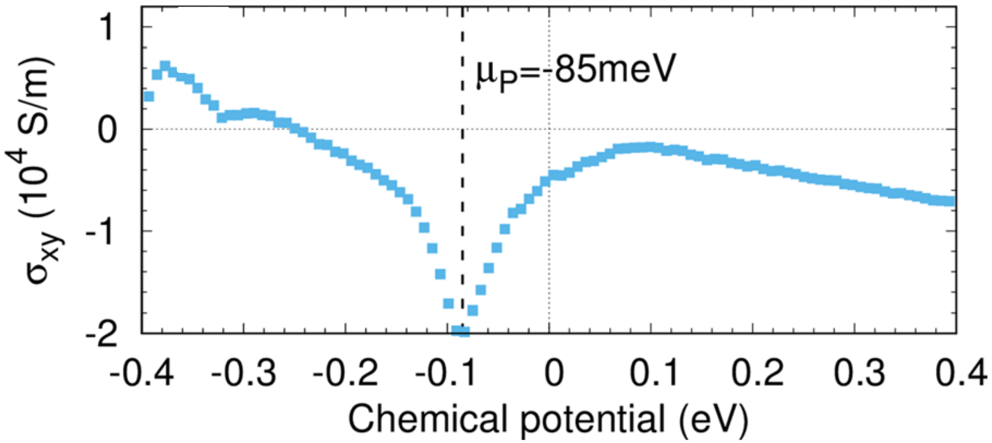

S. Minami, FI, Y.P. Mizuta and M. Saito , Appl. Phys. Lett. **113**, 032403 (2018)

③ FeX_3(X=Al, Ga)

In 2018, two groups discovered Fe-based thermoelectric materials independently.

Ishii Group @ Kanazawa Univ.

2018. Jan.

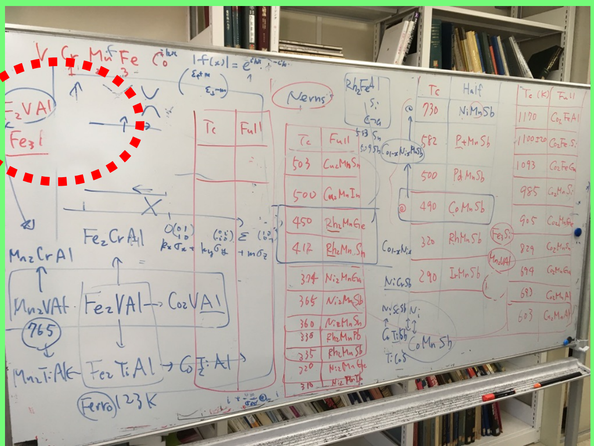

2018. March.

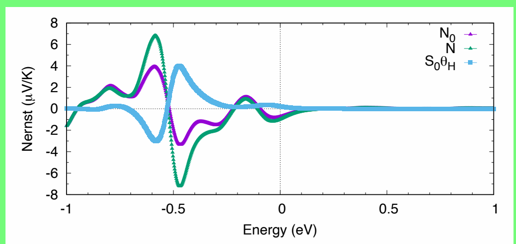

Koretsune and Arita (Tohoku U, Tokyo, Riken)

2018. July
High-throughput calculation,
1400 ferromagnets

Formula	Space group	α_{max} (A K^{-1} m^{-1})	T_c (K)
Fe_3Pt	$Pm\bar{3}m$	6.2	450
Fe_3Ga	$Fm\bar{3}m$	3.0	720
Fe_3Al	$Fm\bar{3}m$	2.7	600
Fe_3Si	$Fm\bar{3}m$	2.5	840
Fe_4N	$Pm\bar{3}m$	2.4	760

……

Nakatsuji Group @ ISSP, Univ. Tokyo

2018. August
Experiments

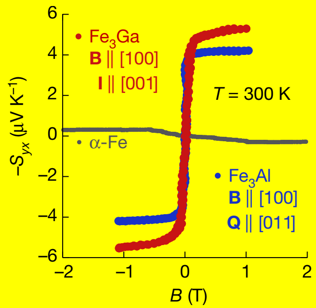

High-throughput calculation for ANE

- Crystal structure: Materials project
- DFT calculation: Quantum Espresso
- Wannier basis: Wannier90

Sakai et al., Nature **581**, 53-57 (2020).
Constructed by Prof. T. Koretsune

crystal structure | DFT calculation & Wannier basis | ANE

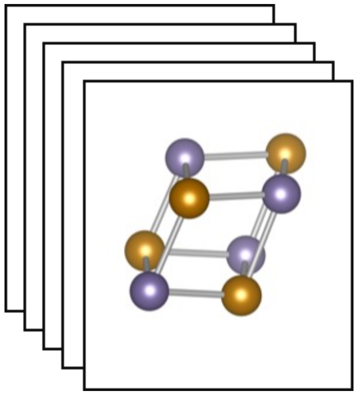

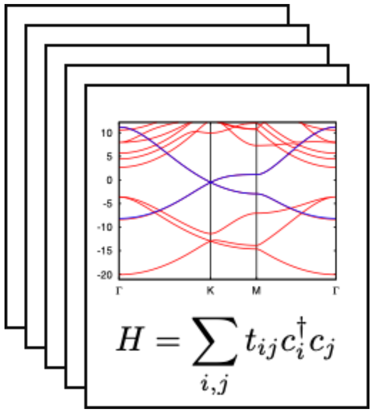

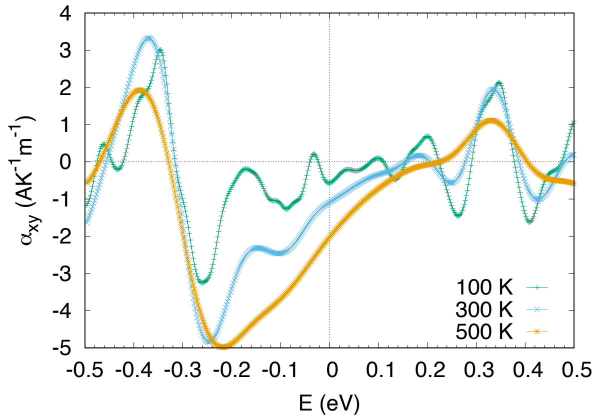

ANE list for ferromagnets

#	unit cell formula	space group	MP-ID	α_{max} (A/Km)
1	Na3 Co1	Fm-3m	mp-1006112	16.44
2	Tl6 Os2	P6_3/mmc	mp-1005760	14.37
3	Pd3 N1	Pm-3m	mp-999292	12.52
4	Cr1 Pd3	Pm-3m	mp-865786	10.54
5	Ni1 Sn1 Rh2	Fm-3m	mp-11519	9.75
6	Rb3 Hf1	I4/mmm	mp-974972	9.334
7	Re1 Pb3	Fm-3m	mp-974611	9.008
8	K6 Co2	P6_3/mmc	mp-976583	8.645
32	Si1 Pd1 O3	Pm-3m	mp-978490	5.672
33	Mn1 Cu2 Sb1	Fm-3m	mp-16320	5.572
34	Mn1 Sb1	Pm-3m	mp-1009207	5.406
35	Sc1 Pd1 O3	Pm-3m	mp-973123	5.342
36	Fe2 C1	P6/mmm	mp-568503	5.331
37	Fe3 Pt1	P4/mmm	mp-11798	5.318
38	Ga1 Fe3	Pm-3m	mp-19870	5.221
39	Fe1 Cu2 Sn1	Fm-3m	mp-21865	5.218
40	Zn1 Ni3	I4/mmm	mp-971804	5.129
41	Fe1 Co2 Si1	Fm-3m	mp-5436	5.124

Fe_3X(X=Al, Ga)

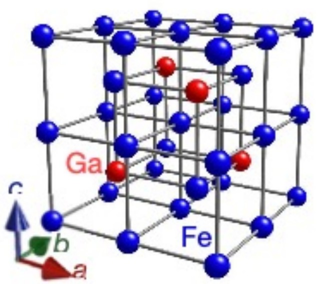

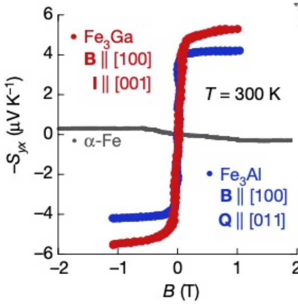

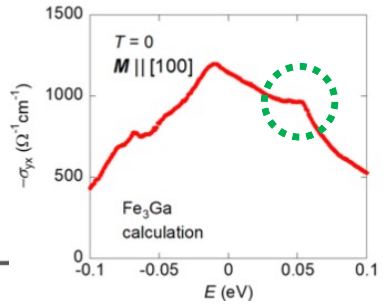

We found new strategy to enhance transverse thermoelectric coefficients

Fe_3Ga

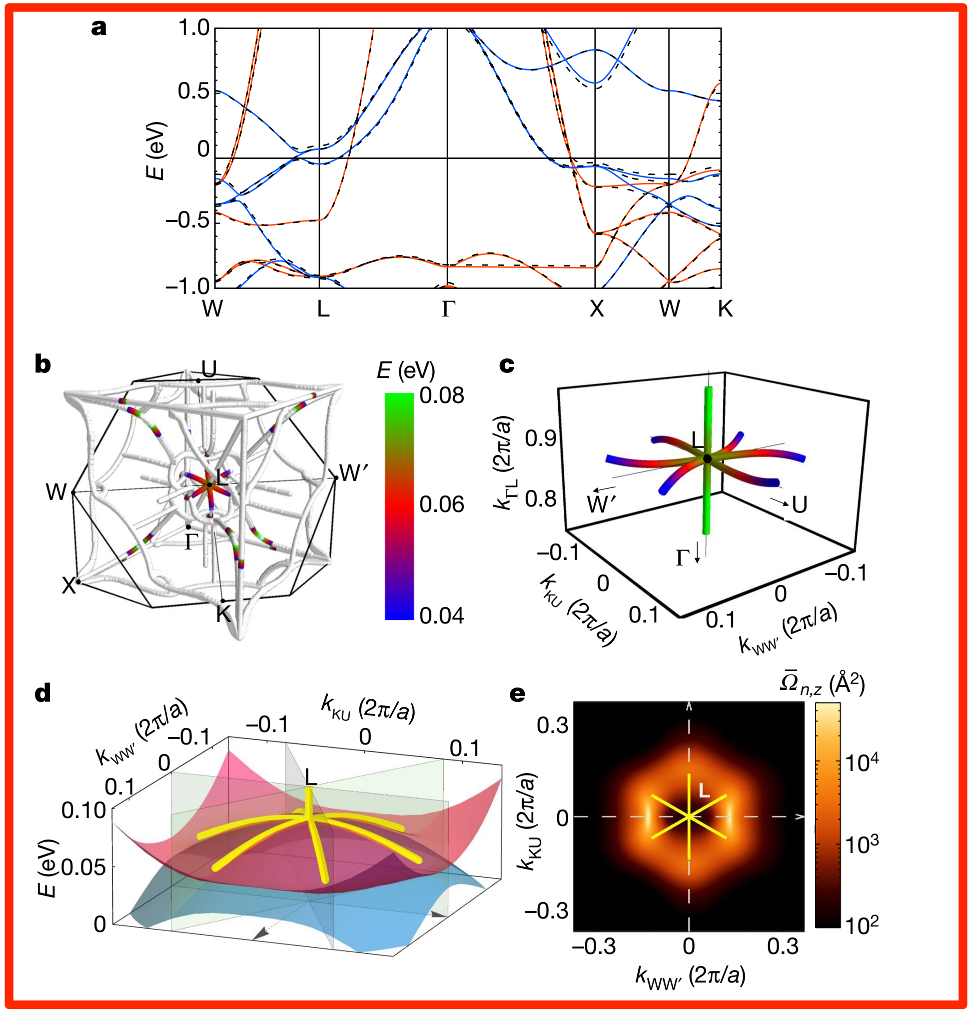

$$\alpha_{yx} = \frac{\pi^2}{3}\frac{k_B^2 T}{|e|}\frac{e^2}{h}\sum_{n,\mathbf{k}} \Omega_{n,z}(\mathbf{k})\delta(E_F - \varepsilon_{n,\mathbf{k}})$$

$$\Omega_{n,\mu\nu} = \mathrm{i}\sum_{n'\neq n} \frac{\langle n \mid v_\mu \mid n'\rangle\langle n' \mid v_\nu \mid n\rangle}{(\varepsilon_n - \varepsilon_{n'})^2}.$$

Small gap structure between eigenvalues (nodal web structure) gave us large curvature of wavefunction

56 | Nature | Vol 581 | 7 May 2020

Nodal line

$$\varepsilon_{n+1}(k_x, k_y, k_z) - \varepsilon_n(k_x, k_y, k_z) = 0$$

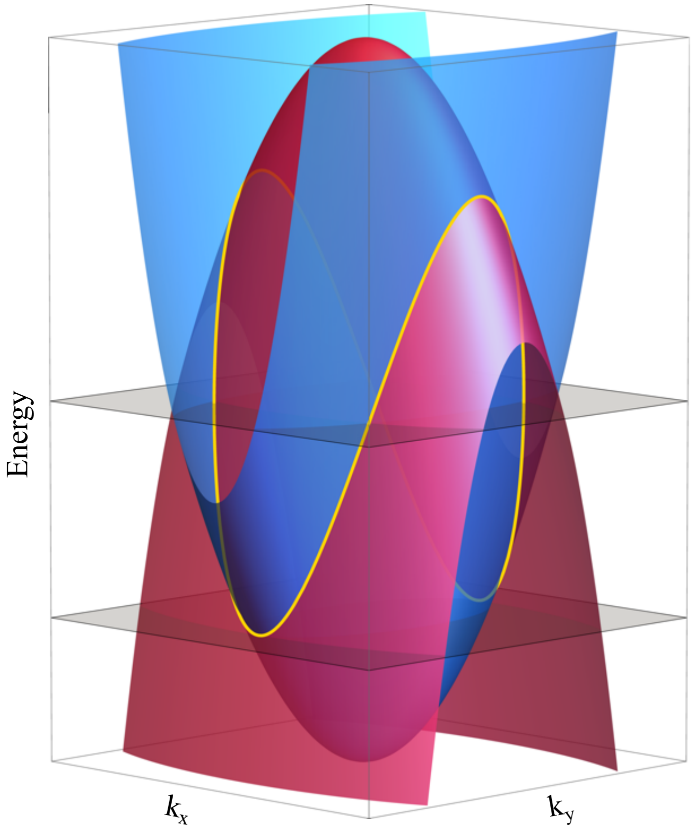

$$\Omega_z^n(\mathbf{k}) = -2\,\mathrm{Im}\sum_{m\neq n}\frac{v_{nm,x}(\mathbf{k})v_{mn,y}(\mathbf{k})}{(\varepsilon_m(\mathbf{k}) - \varepsilon_n(\mathbf{k}))^2}$$

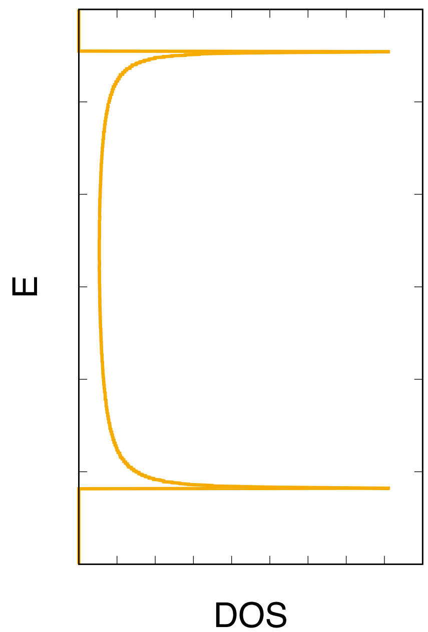

Origin of large ANE

Around L point,

A. Sakai, SM et al., Nature **581**, 53 (2020).

- Nodal lines have flat dispersion. (a)
- Some nodal lines are interconnected. (b)

(a)

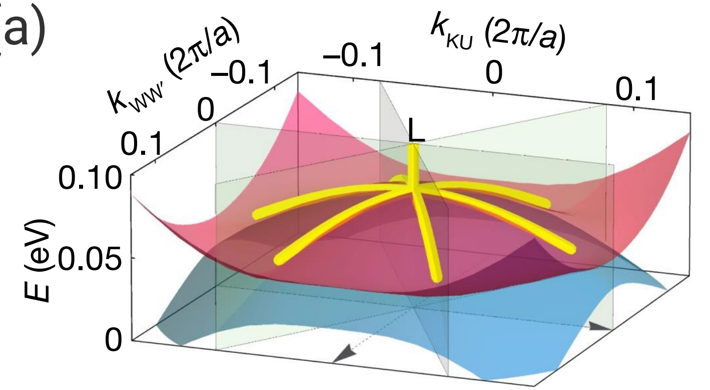

(b)

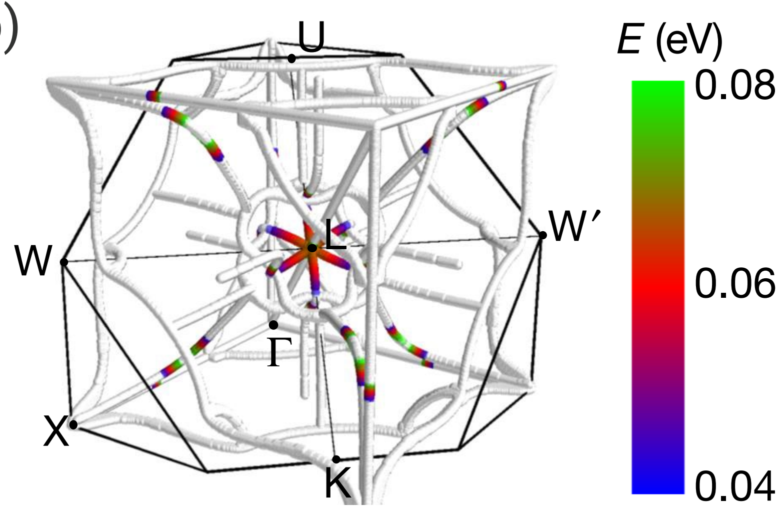

Strong intensity of Berry curvature appears around L point. (c)

(c)

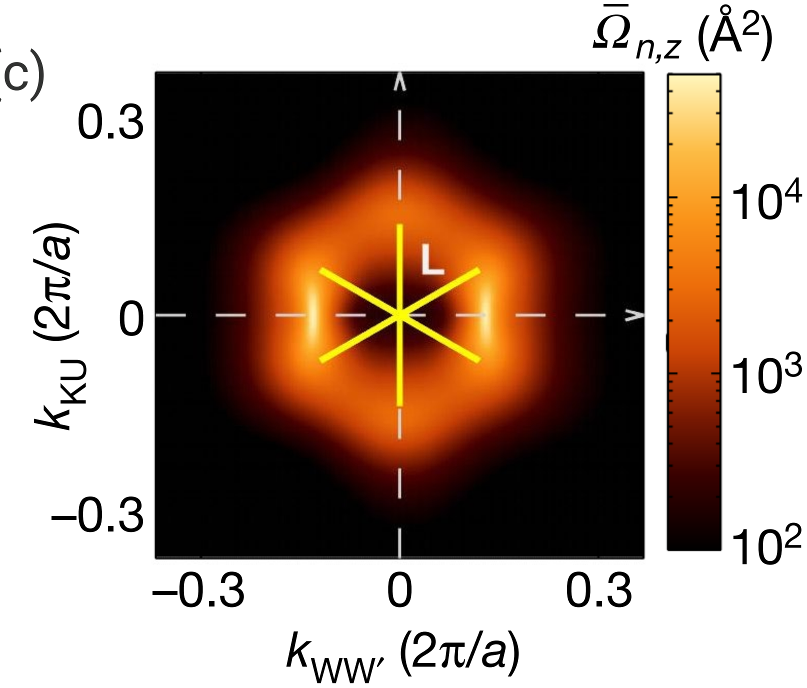

Enhancement of the transverse thermoelectric conductivity originating from stationary points in nodal lines

Susumu Minami *
Department of Physics, The University of Tokyo, Hongo, Bunkyo-ku, Tokyo 113-0033, Japan;
Nanomaterials Research Institute, Kanazawa University, Kakuma, Kanazawa 920-1192, Japan;
and Center for Emergence Matter Science, RIKEN, Hirosawa, Wako, Saitama 351-0198, Japan

Fumiyuki Ishii †
Nanomaterials Research Institute, Kanazawa University, Kakuma, Kanazawa 920-1192, Japan
and Center for Emergence Matter Science, RIKEN, Hirosawa, Wako, Saitama 351-0198, Japan

Motoaki Hirayama
Center for Emergence Matter Science, RIKEN, Hirosawa, Wako, Saitama 351-0198, Japan

Takuya Nomoto
Department of Applied Physics, The University of Tokyo, Hongo, Bunkyo-ku, Tokyo 113-8656, Japan

Takashi Koretsune
Department of Physics, Tohoku University, Sendai, Miyagi 980-8578, Japan

Ryotaro Arita
Center for Emergence Matter Science, RIKEN, Hirosawa, Wako, Saitama 351-0198, Japan
and Department of Applied Physics, The University of Tokyo, Hongo, Bunkyo-ku, Tokyo 113-8656, Japan

(Received 14 September 2020; revised 2 November 2020; accepted 3 November 2020; published 23 November 2020)

Motivated by the recent discovery of a large anomalous Nernst effect in Co_2MnGa, Fe_3X (X=Al, Ga) and $Co_3Sn_2S_2$, we performed a first-principles study to clarify the origin of the enhancement of the transverse thermoelectric conductivity α_{ij} in these ferromagnets. The intrinsic contribution to α_{ij} can be understood in terms of the Berry curvature Ω around the Fermi level, and Ω is singularly large along nodal lines (which are gapless in the absence of the spin-orbit coupling) in the Brillouin zone. We find that not only the Weyl points but also stationary points in the energy dispersion of the nodal lines play a crucial role. The stationary points make sharp peaks in the density of states projected onto the nodal line, clearly identifying the characteristic Fermi energies at which α_{ij} is most dramatically enhanced. We also find that α_{ij}/T breaks the Mott relation and show a peculiar temperature dependence at these energies. The present results suggest that the stationary points will give us a useful guiding principle to design magnets showing a large anomalous Nernst effect.

DOI: 10.1103/PhysRevB.102.205128

Analysis for ANE based on nodal line

S. Minami, **FI**, et al., Phys. Rev. B, **102**, 205128 (2020).

- Nodal line will be a source of large Berry curvature.
  - Nodal line: the degenerated states of some bands. $\Delta\varepsilon(\mathbf{k}) \equiv \varepsilon_n(\mathbf{k}) - \varepsilon_m(\mathbf{k}) = 0$
- Introduce a simple assumption by Ω_{NL} and D_{NL}:

$$\frac{\partial \sigma_{ij}}{\partial \varepsilon} = \varepsilon_{ijl} \sum_{n\boldsymbol{k}} \Omega_{n,l}(\boldsymbol{k}) \delta(\varepsilon - \varepsilon_{n\boldsymbol{k}}), \\ \sim \Omega^{n}_{\mathrm{NL}}(\varepsilon) D^{\mathrm{SO},n}_{\mathrm{NL}}(\varepsilon) + \Omega^{n+1}_{\mathrm{NL}}(\varepsilon) D^{\mathrm{SO},n+1}_{\mathrm{NL}}(\varepsilon).$$

$$\frac{\partial \sigma_{ij}}{\partial \varepsilon} \sim \Omega^{n}_{\mathrm{NL}}(\varepsilon)\left[D^{\mathrm{SO},n}_{\mathrm{NL}}(\varepsilon) - D^{\mathrm{SO},n+1}_{\mathrm{NL}}(\varepsilon)\right].$$

Peak of D_{NL} can be a mechanism of large ANE.

Nodal line for $Co_3Sn_2S_2$

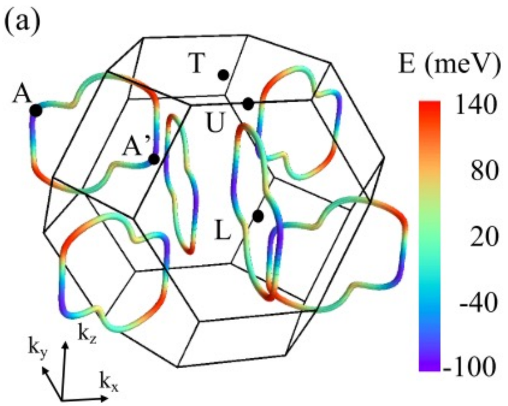

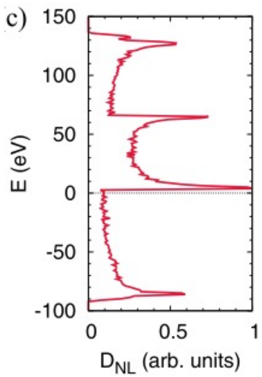

Density of states for NL can be express the trend of ANE.

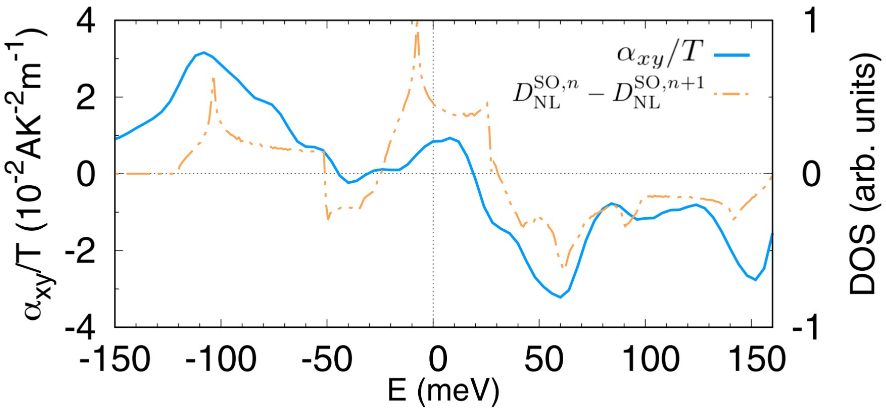

Summary Part I

1. Which contribution is dominant in real materials?
   👉 N_0 might be dominant in many magnetic metals
   Seebeck-driven term $r_H S_0$ in Chern insulating system
2. What is the key to enhancing the Nernst coefficient?
   👉 Berry curvature and Sharp DOS, singularity
   Nodal line DOS, vHSs are important
   👉 2D Materials!

3. Can we predict the behavior of the Nernst effect?
   👉 We need more application studies
   👉 Scattering and correlation effect on relaxation time

$$N = \frac{N_0}{1 + r_H^2} - \frac{r_H S_0}{1 + r_H^2}$$

Applications
Part II

Collaborators
Y. Zhang, R. Syariati,
and N. Yamaguchi

High-throughput Calculation Schemes

- We divide the scheme into the automated calculation and present the data.
- The database has a role as an interface between calculation and showing the data
- The initial and final data will save in the database
- The calculation result will show on the web server

Strategy for selecting 2D Magnetic Materials

- Experimentally synthesized
- Replace the atom according to the experimentally synthesized structures
- From the publication of both the experiment and theoretical paper
- Make a 2D system from the existing layered structure
- From existing 2D database

Web Server Database Screenshot

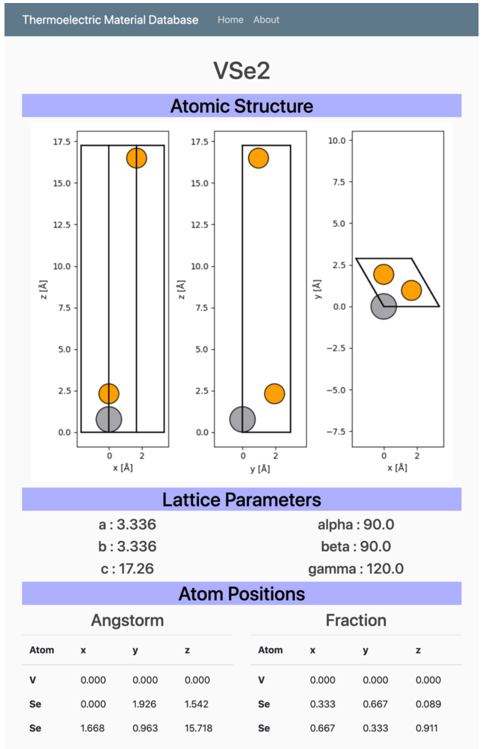

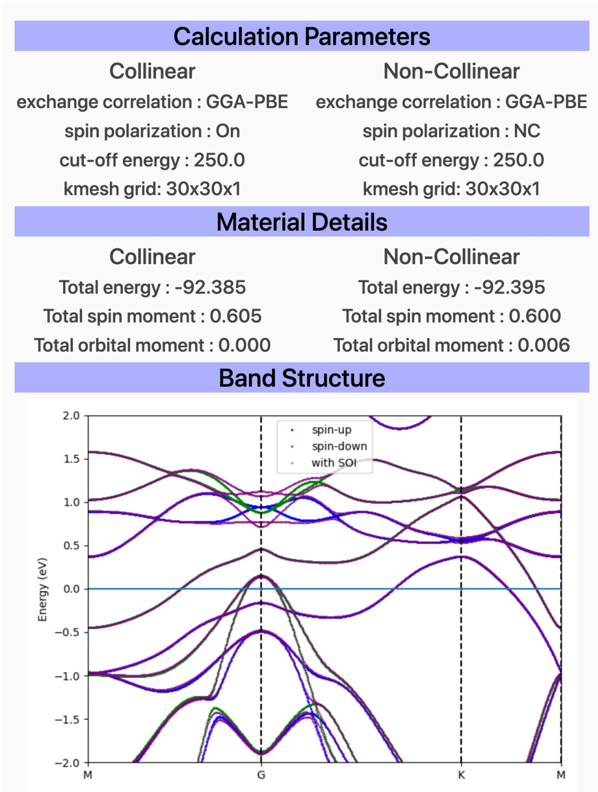

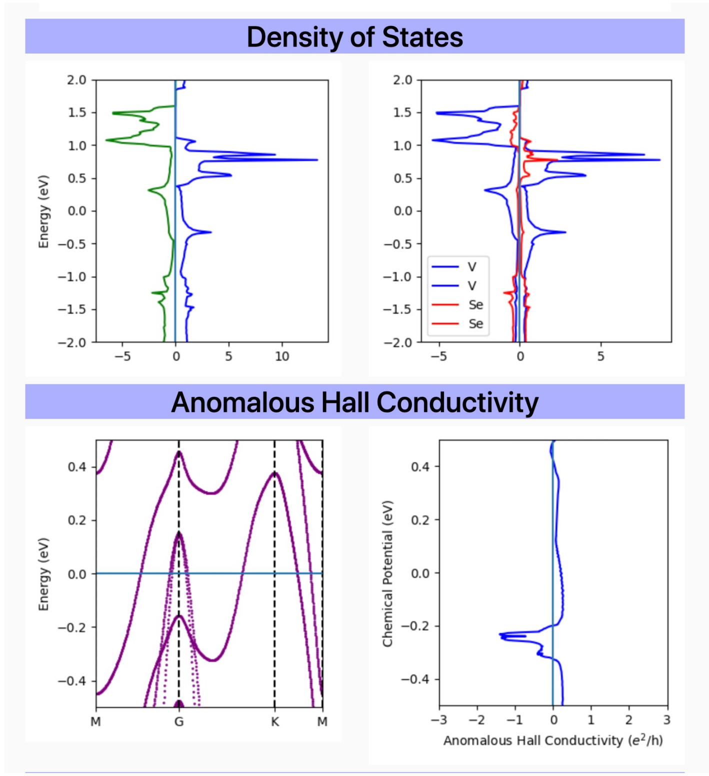

Anomalous Hall Effect Materials

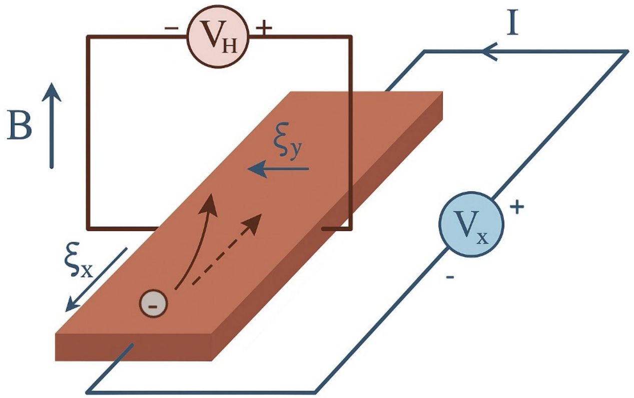

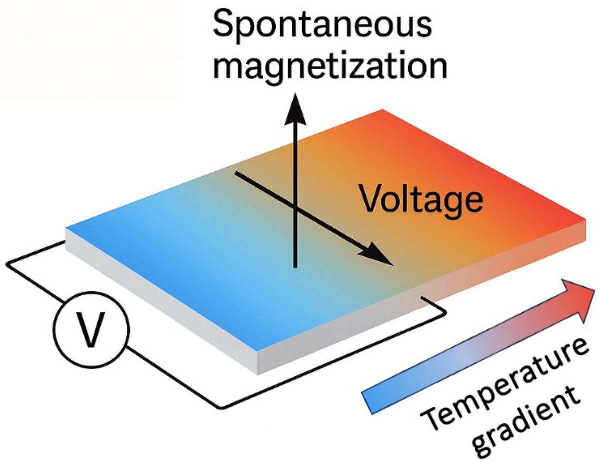

- The Anomalous Hall Effect (AHE) is vital for applications in spintronics and thermoelectric materials.

- When current flows in a material exhibiting AHE, charge carriers deflect laterally, resulting in a transverse voltage even in the absence of an external magnetic field.

- When a temperature gradient is applied to these materials, a voltage is generated in the vertical direction, which efficiently converts waste heat into useful electricity.

2D Structures database

Current Calculated 2D Structures

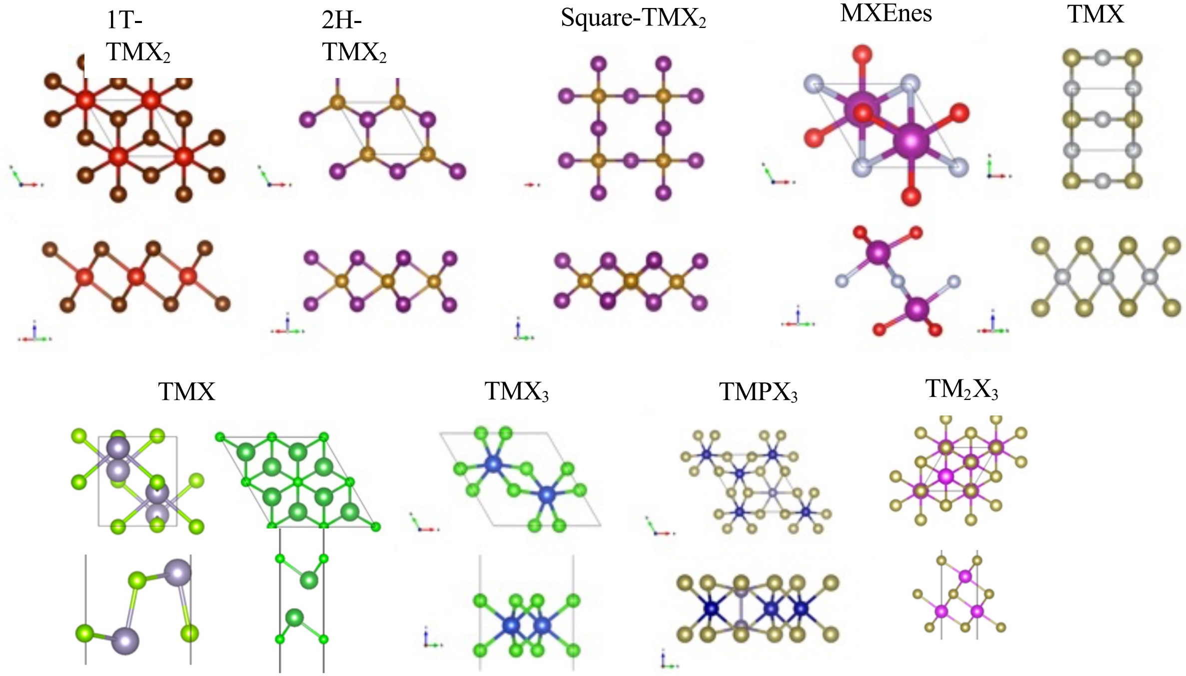

- To systematically search for materials that exhibit a strong AHE, we used OpenMX to build a high-throughput database specialized for 2D magnetic materials.
- A total of 4,400 structures have been calculated to date, of which 3,589 are magnetic.
- In addition, by using OMXsigmaxy, we calculated the anomalous Hall conductivity (σ_{xy}) for a total of 2,526 structures, and also analyzed the density of states (DOS) and band structure for approximately 1,186 of these structures.

Workflow for the computation of anomalous Hall conductivity

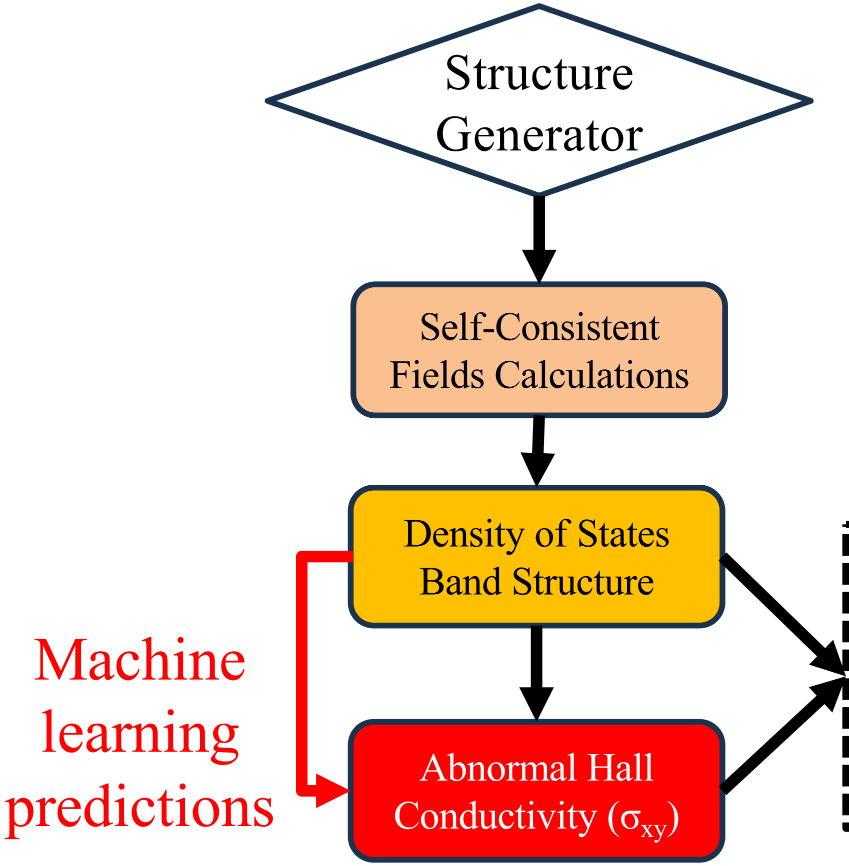

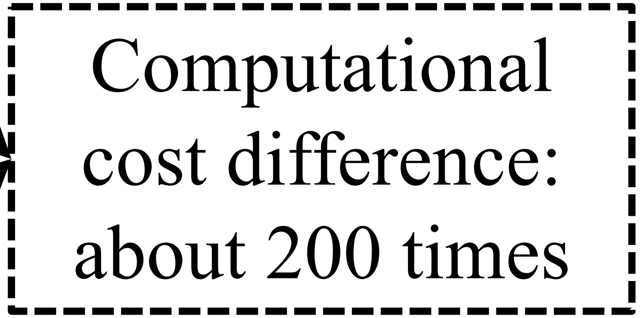

- The computational cost of $\sigma_{x\gamma}$ is hundreds of times higher than that of density of states or band structure calculations, making it impractical for large-scale materials exploration.

- To address this challenge, we use machine learning to identify materials that may have high $\sigma_{x\gamma}$, reducing the need for exhaustive first-principles calculations.

Physical inspire feature engineering :DOS

Kubo formula:

$$\Omega_z^n(k) \propto \sum_{n' \neq n} \frac{\mathrm{Im}\left[\langle n|v_x|n'\rangle\langle n'|v_y|n\rangle\right]}{(\epsilon_{n'} - \epsilon_n)^2},$$

$$\sigma_{xy} = -\frac{e^2}{\hbar}\int \frac{d^3k}{(2\pi)^3}\sum_n f_n(k)\ \Omega_z^n(k)$$

DOS features inspired by the Berry curvature representation:

Difference of spin-polarized DOS and its slope ($D_{\text{diff}}(\epsilon)$, $D'_{\text{diff}}(\epsilon)$):
Characterize spin splitting, which affects the occupation function $f_n(k)$ and thus determines which Berry curvatures Ω_z^n contribute to σ_{xy}.

Total DOS and its slope ($D_{\text{sum}}(\epsilon)$, $D'_{\text{sum}}(\epsilon)$):
Describe the density and sharpness of states near Fermi surface, influencing the interband velocity matrix elements $\langle v_x\rangle$, $\langle v_y\rangle$ in the numerator.

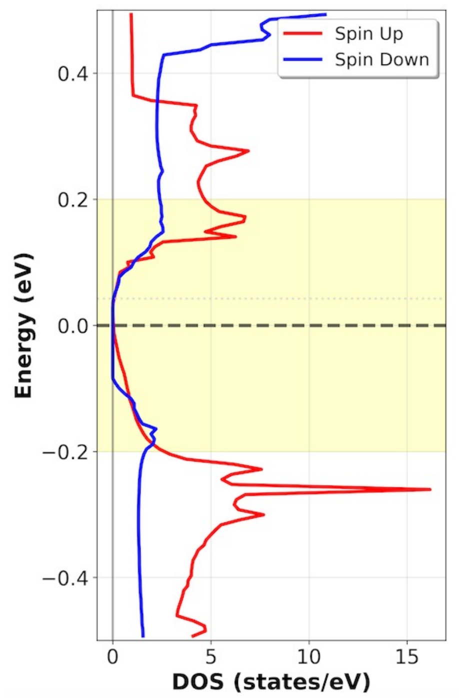

Physical inspire feature engineering : band structure

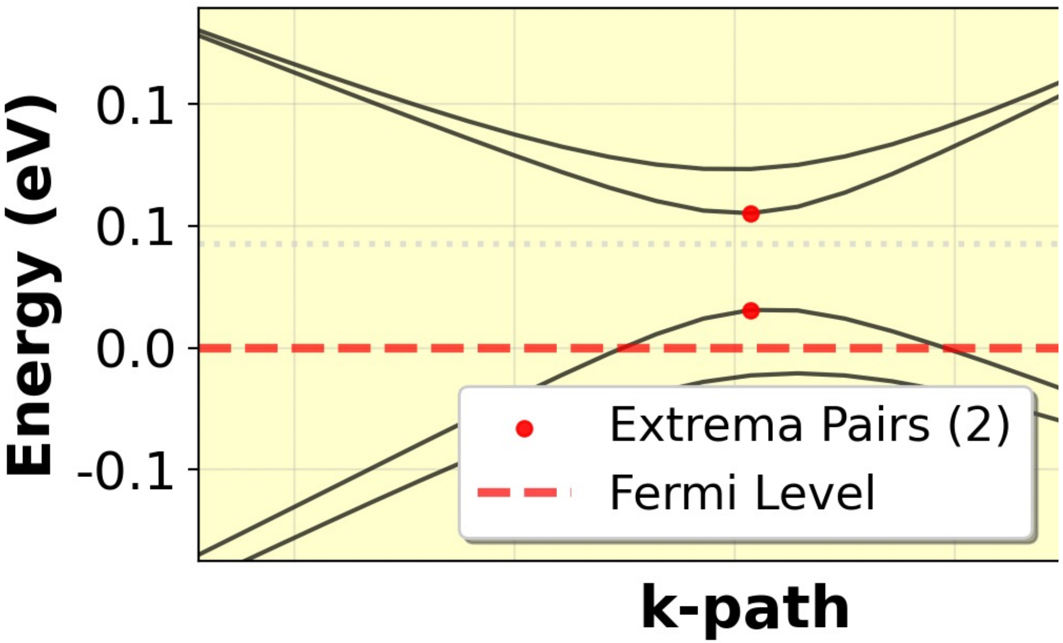

SOC-induced gap (ΔE_{deg}):

Represents the energy separation $(\boldsymbol{\epsilon}_{\boldsymbol{n}'} - \boldsymbol{\epsilon}_{\boldsymbol{n}})^2$ in the denominator. Smaller gaps lead to stronger Berry curvature peaks.

Gap center energy (E_{center}):

Indicates whether a SOC-induced gap lies near Ferni surface, affecting whether its associated $\Omega_z^n(\boldsymbol{k})$ is included via $f_n(\boldsymbol{k})$.

Band velocity (v_{deg}):

Measures the dispersion near avoided crossings. Larger velocity enhances the numerator $\langle n\,|v_x|\,n'\,\rangle\langle n'\,|v_y|\,n\,\rangle$.

These features can be represented as a vector: $(x_1, x_2 \ldots x_i)$, where i is number of the features, x can be v_{deg}, ΔE_{deg} etc.

Kernel Mean Embedding for fixed-length vector representation

- However, such features are not fixed across materials, leading to **inconsistent feature vector lengths**, which are difficult for standard machine learning models to handle.
- In this study ,we use Kernel Mean Embedding (KME), a method that transforms data distribution into a **fixed-length vector representation**.
- For each physical feature the KME vector is computed as:

$$\phi_j = \frac{1}{n}\sum_{i=1}^{n} \exp\left(-\frac{(x_i - g_j)^2}{2\gamma^2}\right)$$

x_i: a raw sample value.
g_j : the j-th point on a uniform grid covering all feature values.
γ: the kernel width, controlling smoothness.
ϕ_j: the resulting KME vector component at grid point g_j.

Kernel Mean Embedding for fixed-length vector representation

The left figure shows an illustration of KME.

For comparison, the right figure shows a conventional summary statistical descriptor.

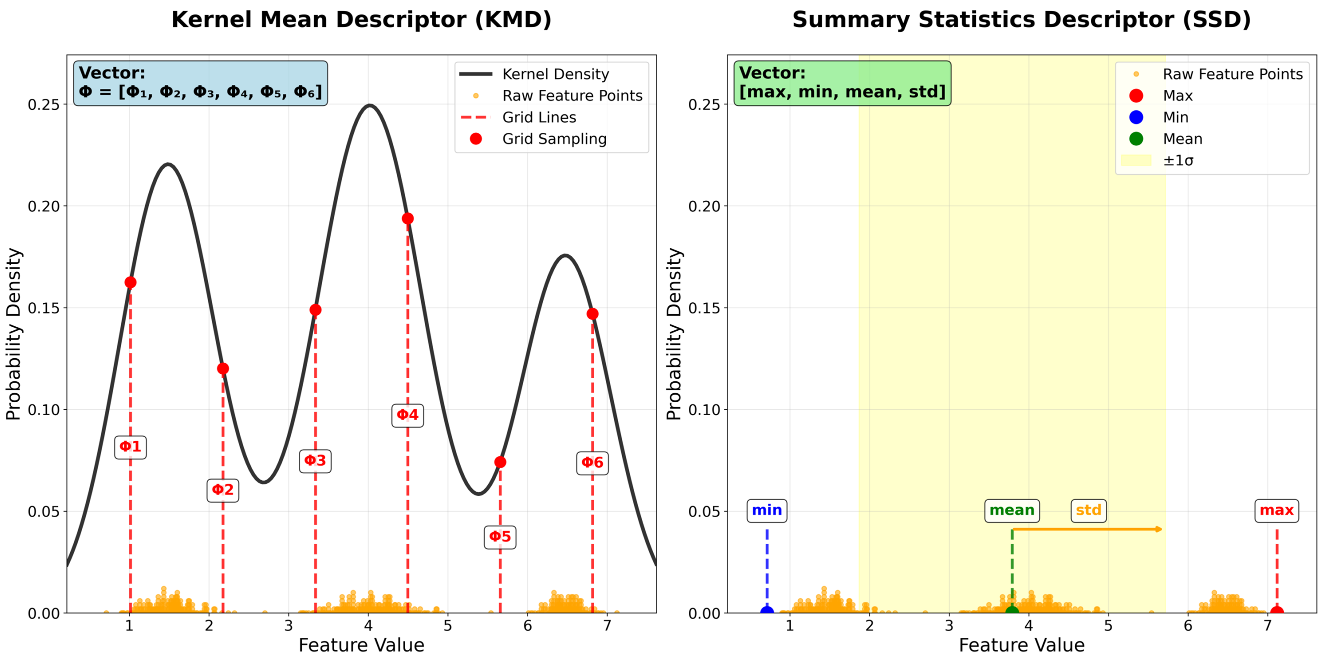

Kernel Mean Embedding for fixed-length vector representation

This study (Random forest with KME as input)

Raw data of DOS and band structure

Feature engineering

KME vector:

$$\Phi = [\Phi_1, \Phi_2, \Phi_3, \Phi_4, \Phi_5, \Phi_6]$$

As input

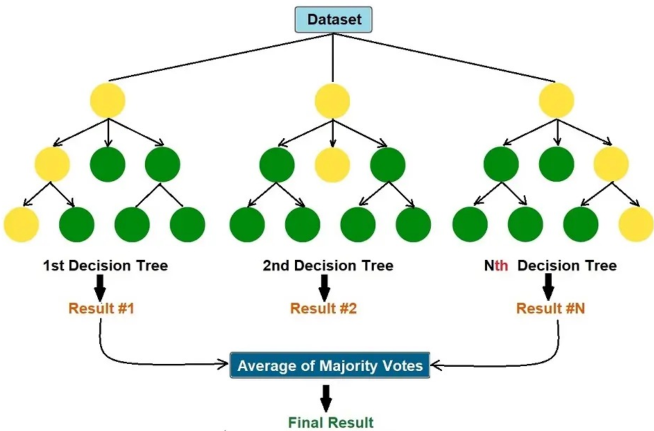

Baseline (Deep learning)

Raw data of DOS and band structure

Convolutional Neural Network (CNN)

Final Result

Crystal Structures

Crystal Graph Convolutional Neural Network (CGCNN)

Final Result

Classification performance of different models
Max $\sigma_{xy} > 0.5\ e^2/h$ or not (between Fermi level -0.1 eV to 0.1 eV)

- We use **Accuracy (ACC)** to measure correct predictions under a fixed threshold (50 %), and **AUC** to evaluate how well the model ranks high-σ_{xy} materials across all thresholds. (266 low, 431 high)
- The **KME** model achieves the best results (ACC: 78.6%, AUC: 82.8%), and the simple, physically grounded **SSD** also performs competitively (AUC: 80.9%).
- Deep learning baselines like **DOS_CNN** (using density of states) and **CGCNN** show lower AUCs (76.9% and 68.1%), due to their limited ability to capture AHE-relevant features.
- These results demonstrate that physically informed feature engineering outperforms end-to-end learning in predicting quantum transport properties, especially with limited data.

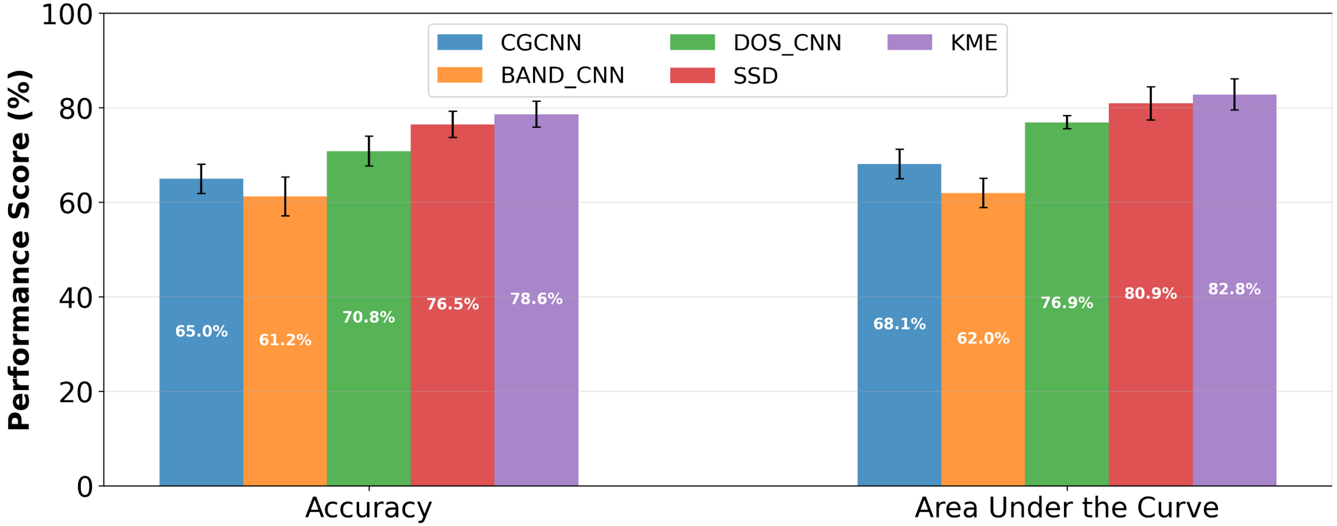

Confusion Matrix

True Positive (High - High):
The actual label is High, and the model predicted High.

False Negative (High - Low):
The actual label is High, but the model predicted Low.

False Positive (Low - High):
The actual label is Low, but the model predicted High.

True Negative (Low - Low):
The actual label is Low, and the model predicted Low.

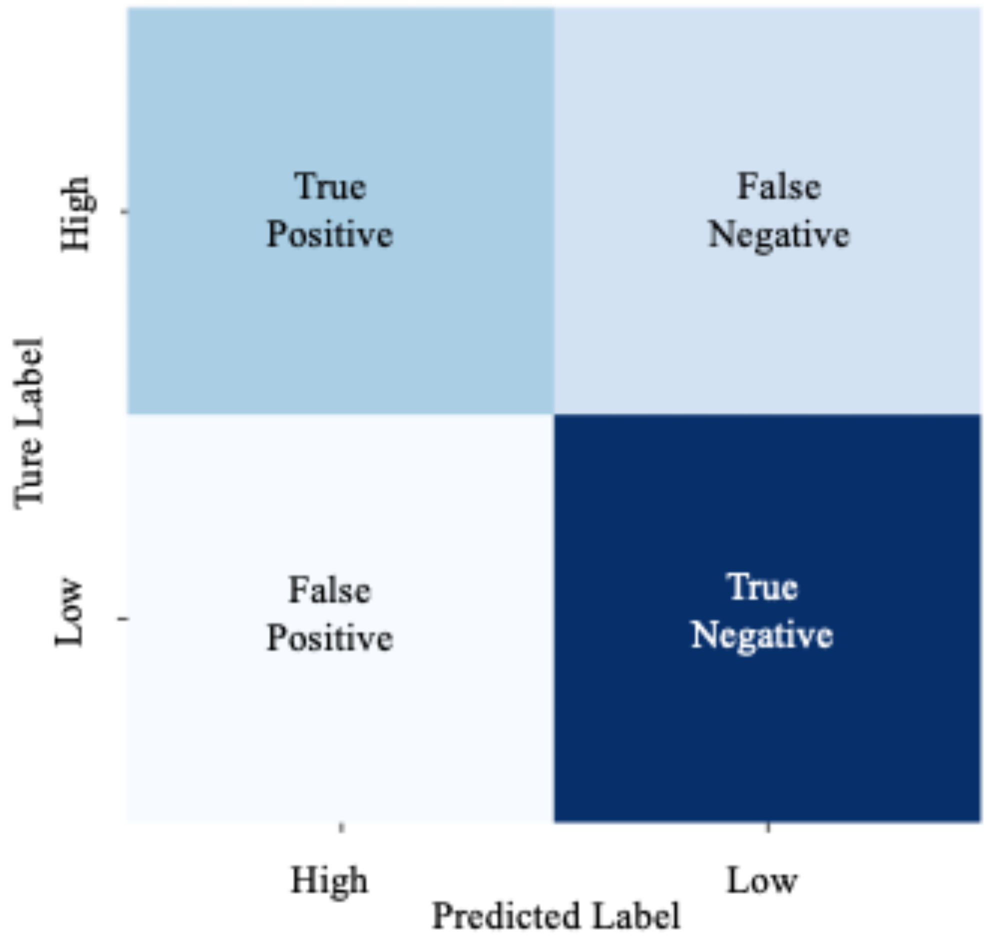

SHAP analysis for true positive case TaCl

- We use **SHAP (SHapley Additive exPlanations)** to interpret model predictions by quantifying the contribution of each feature to the final output.
- For the **true positive** case (TaCl), the predicts high σ_{xy} ,primarily due to the **extremum pairs near the Fermi level**, leading to the highest SHAP contribution from $\boldsymbol{E}_{\mathbf{center}}$.
- Additionally, a **sharp change in DOS spin splitting at ~0.1 eV** contributes positively via $\boldsymbol{D}'_{\mathbf{diff}}(\boldsymbol{\epsilon})$**.**
- These attributions align well with the physical origin of Berry curvature, confirming that the model captures essential AHE-driving mechanisms.

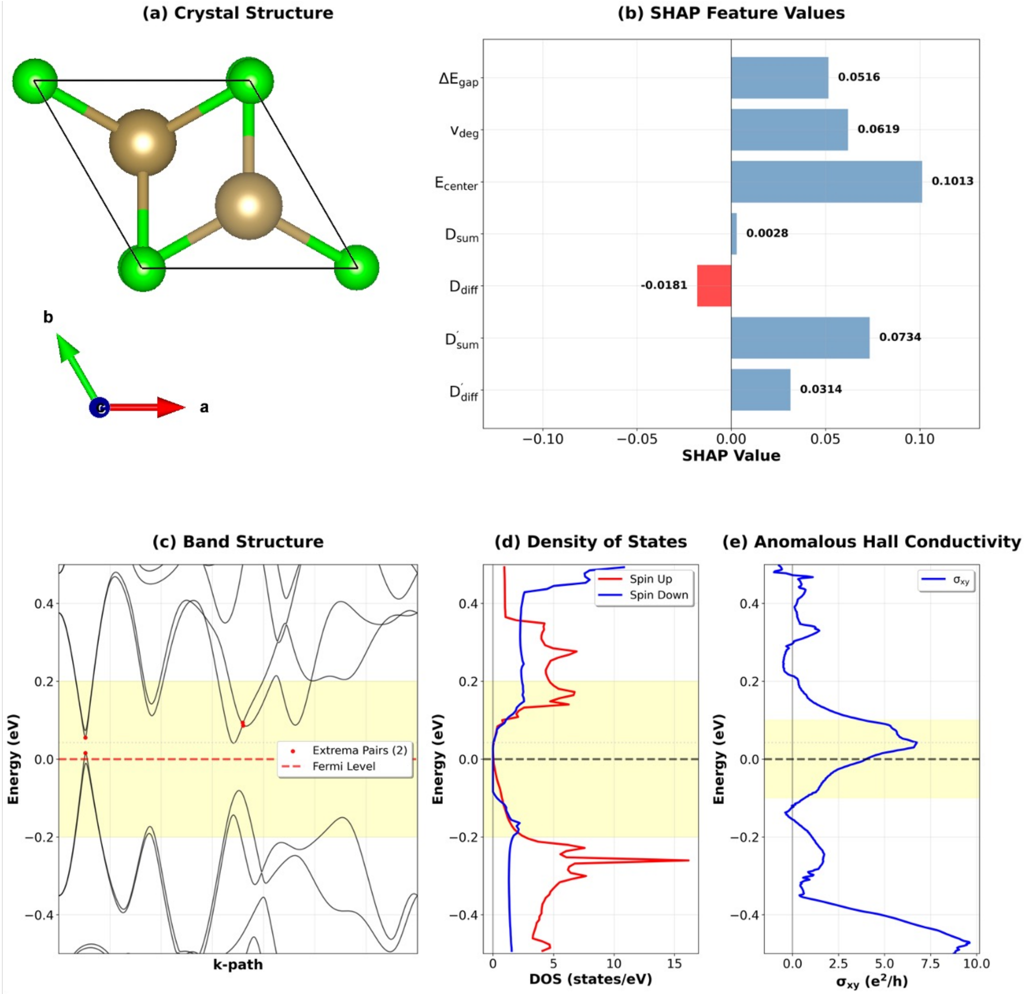

SHAP analysis for true negative case MnOSe

- SHAP analysis shows that **all band-derived** contribute negatively, as **no** SOC-induced gaps are found near the Fermi level.
- While the DOS shows **minor spin splitting**, the SHAP contribution from $\boldsymbol{D_{\text{diff}}(\epsilon)}$ is small.
- The only weakly positive contribution comes from total DOS magnitude $\boldsymbol{D_{\text{sum}}(\epsilon)}$,but it is outweighed by dominant negative signals.
- As a result, the model confidently predicts low σ_{xy} consistent with the **lack of relevant physical mechanisms** for the AHE in this material.

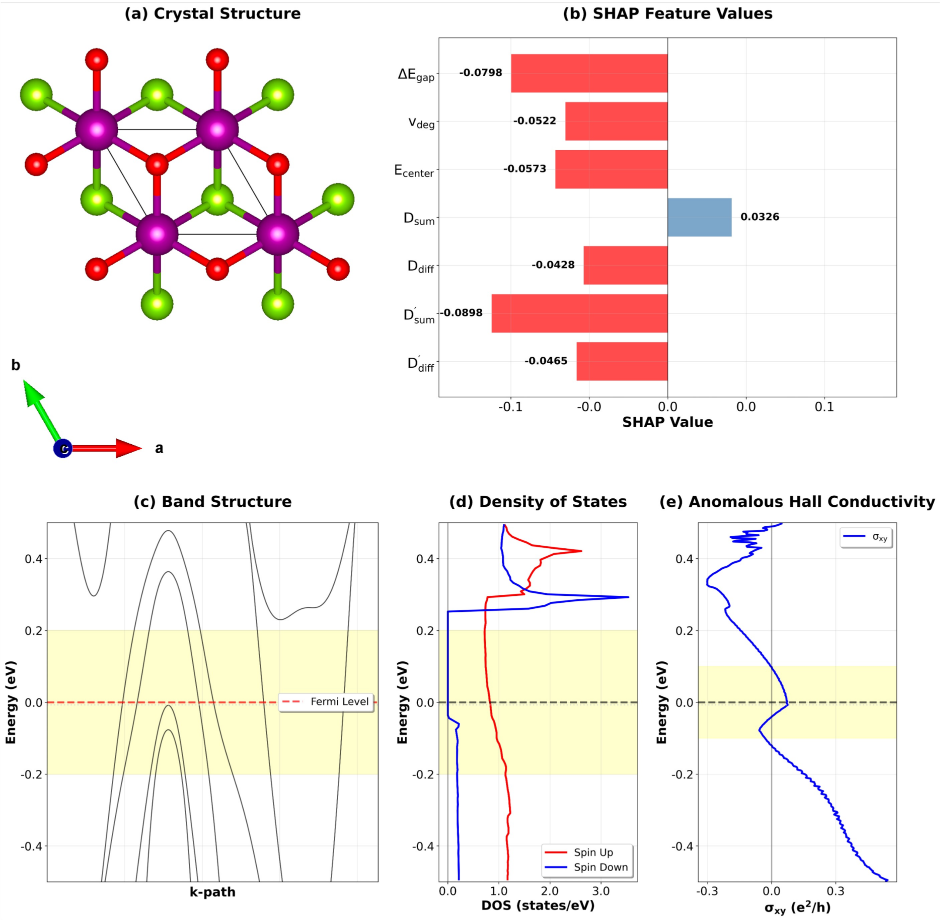

SHAP analysis for false positive case $FePSe_3$

- $FePSe_3$ is a false positive where the model predicts high σ_{xy} due to strong positive SHAP values from DOS-based features, such as spin polarization and spectral gradient.
- However, band-derived features contribute negative SHAP values, correctly indicating the absence of SOC-induced gap.
- The model is misled by local DOS features but lack supporting band topology.
- This case highlights a failure mode where **high DOS-derived SHAP values override negative contributions from band features,** resulting in an overestimation of AHE.

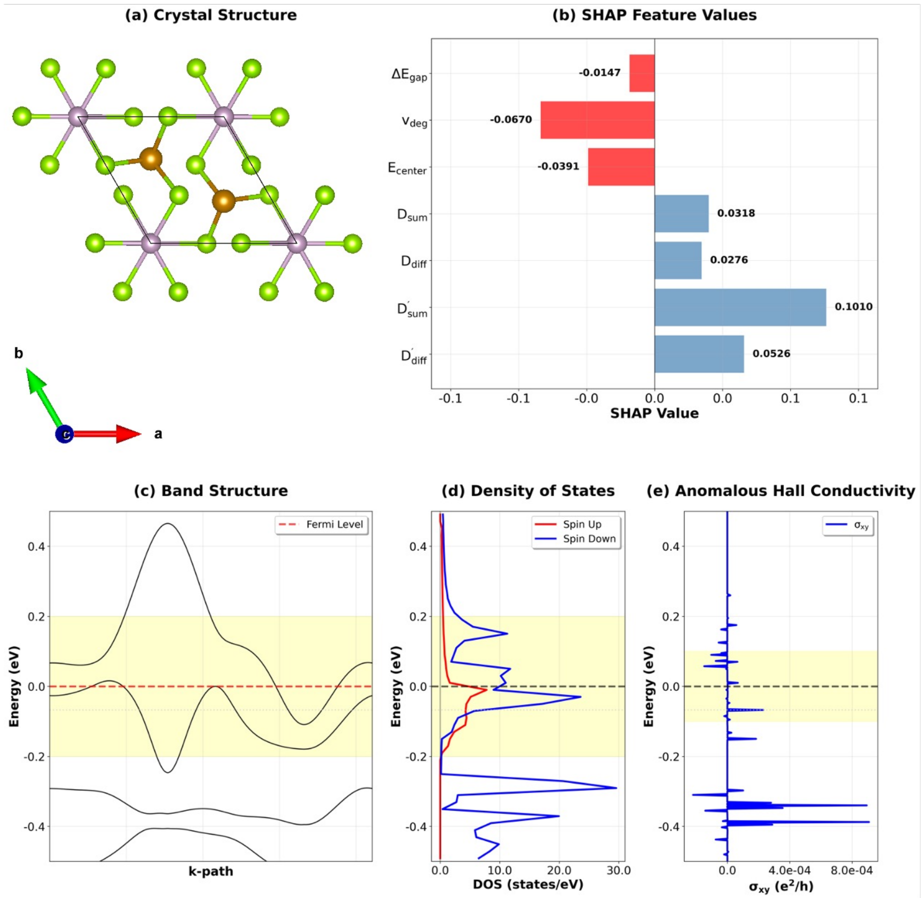

SHAP analysis for false negative case RuS_2

- RuS_2 is a false negative where the model underestimates σ_{xy} despite strong positive SHAP values from DOS-based features like spin polarization and DOS slope.
- Band-derived features have negative SHAP values, due to the absence of clear SOC-induced gap.
- The model's decision is dominated by the lack of band-based indicators, leading to a low prediction score.
- This case mirrors the false positive failure mode, highlighting how insufficient band signals can suppress true AHE responses even when DOS features are strong.

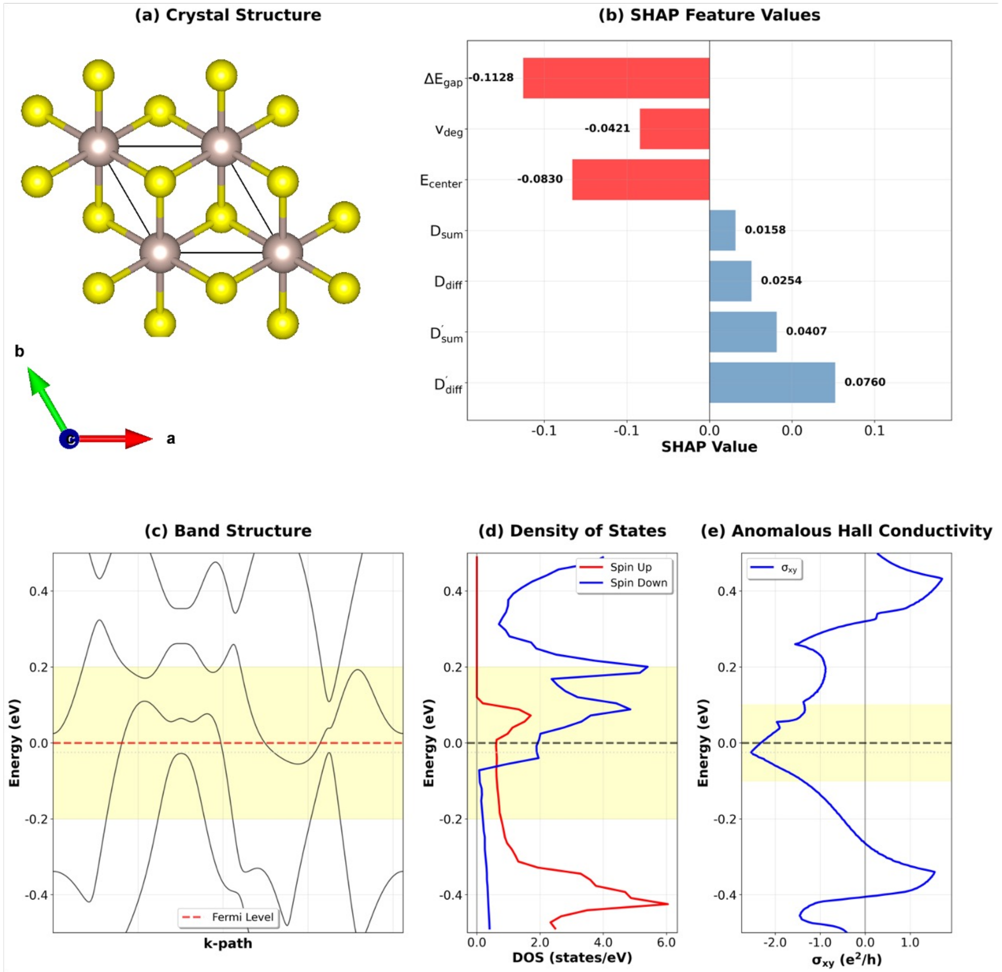

Part II Summary

- Developed a physically interpretable machine learning framework to predict anomalous Hall conductivity in 2D magnetic materials using Kernel Mean Embedding of electronic structure features.

- Transformed variable-length descriptors, such as spin-resolved DOS, SOC-induced band gaps, and local band velocities, into fixed-length KME vectors compatible with ML models.

- Achieved superior classification performance (AUC: 82.8%) compared to deep learning baselines (e.g., CGCNN, CNNs), demonstrating the effectiveness of physics-driven feature engineering.

- SHAP interpretability analysis identified key physical contributors to AHE, and revealed typical failure modes via case studies (FP and FN).

- The framework enables efficient, interpretable high-throughput screening of AHE materials and can be extended to other topological or spintronic material discovery tasks.

- In the future, we aim to go beyond high-symmetry paths and incorporate full Brillouin zone information to capture key topological features like Weyl points, enabling more accurate and generalizable predictions of AHE materials.